applied sciences

MDPI

Article

Uneven Stiffness Coal Seam: A New Structural Factor Prone to Coal Burst Based on Stiffness Theory

Tiewu Tang [1,2,*], Zhigang Deng [2], Weiguang Ren [1,2], Shankun Zhao [2], Yin Wang [2], Yang Zhao [2] and Wenxin Li [3,*]

1 Chinese Institute of Coal Science, Beijing 100013, China; rwgjszsj@outlook.com
2 China Coal Research Institute, Beijing 100013, China; dengzhigang2004@163.com (Z.D.); zhaoshankuncom@163.com (S.Z.); wingtongwing@hotmail.com (Y.W.); zhao_no1@126.com (Y.Z.)
3 State Key Laboratory of Strata Intelligent Control and Green Mining Co-Founded by Shandong Province and the Ministry of Science and Technology, Qingdao 266590, China
* Correspondence: ykttw@163.com (T.T.); li17753299337@163.com (W.L.)

Abstract: The development of stiffness theory is constrained by its contradiction with engineering experience. Several easily overlooked details of stiffness theory were clarified, and a qualitative evaluation formula for the risk of coal burst was provided. Then a novel structure factor called uneven stiffness coal seam structure (USCS), which consists of high stiffness zone (HSZ), low stiffness zone (LSZ), and contiguous roof and floor, was proposed. Many areas prone to coal bursts, such as thinning zones, bifurcating areas, magmatic intrusion areas, and remnant pillar affected areas of coal seam, are the HSZs of USCSs. Comparative analysis of the uneven stiffness coal seam under different roof conditions and examination of the simplified trisection model of the USCS were conducted. Then 6 groups of 14 simplified 2D models using COMSOL5.2 was constructed based on controlled variable method to simulate different responses of the USCS with varying parameters under same working conditions. The results demonstrate the following: (1) coal bursts occur only when both the failure criterion and the stiffness criterion are simultaneously satisfied, the risk of coal burst (r_{CB}) is the product of the risk of failure (r_F) and the risk of instability (r_I). (2) The pressure concentration function of USCS facilitates stress concentration from LSZ to HSZ, thus raising the r_F in HSZ. The stiffness reduction function of USCS reduces the local mine stiffness (LMS) of the HSZ, allowing the system to meet the stiffness criterion even with a hard roof, thereby raising the r_I in HSZ and reconciling the contrast between stiffness theory and engineering experience. Failures within HSZ of the USCS enables the roof strata to release bending deformation energy without roof breakage. (3) The normal stress of HSZ is positively correlates with the value of $E_R H_R K_H S_L / K_L S_H$; The LMS of the HSZ is positively correlated with the value of $E_R K_L / K_H H_R S_L S_H$. The USCS boasts significant advantages in integrating and harmonizing various existing theories and explaining multiple specific types of coal bursts. By applying relevant USCS findings, new explanations can be provided for engineering phenomena such as the time-delayed coal bursts, the inefficient pressure relief in ultra thick coal seams, and the "microseism deficiency" observed prior to certain coal bursts.

Keywords: coal burst; stiffness theory; LMS; failure criterion; USCS; HSZ; LSZ; NSC

check for updates

Citation: Tang, T.; Deng, Z.; Ren, W.; Zhao, S.; Wang, Y.; Zhao, Y.; Li, W. Uneven Stiffness Coal Seam: A New Structural Factor Prone to Coal Burst Based on Stiffness Theory. *Appl. Sci.* **2024**, *14*, 24. https://doi.org/10.3390/app14010024

Academic Editor: Jan Yperman

Received: 25 October 2023
Revised: 7 December 2023
Accepted: 13 December 2023
Published: 19 December 2023

1. Introduction

Coal burst, also known as coal bump or rock burst, is a dynamic phenomenon arising from the rapid release of stored elastic energy within the coal and rock mass around the mining space [1–3]. This phenomenon manifests suddenly, accompanied by fragments ejection or rapid deformation of roadway, generating load noise and air blasts, and often resulting in significant damage [4–6]. Undoubtedly, coal burst is a paramount dynamic hazard, posing a serious threat to the safety of coal mine production.

Researchers proposed many kinds of theory, such as strength theory [7], energy theory [8], stiffness theory [9–12], bursting liability theory [13], instability theory [14], catastrophe theory [15–17], the "three-factors" mechanism [18], the rock burst start-up mechanism [19], the dynamic and static combined load-induced mechanism [20], and the disturbance response instability mechanism [21], to clarify the mechanism underlying coal burst. Although so many progress have been made in understanding coal burst mechanisms, there is still no universally accepted theory within the academica [22]. The stiffness theory merits particular attention among the various mechanisms of coal burst due to its evident advantages and disadvantages.

The stiffness theory originated from the research on the influence of testing machine stiffness on the bursting intensity of rock specimen failure. Cook emphasized the resemblance between the unstable failure of specimens on low-stiffness test machines and rock burst incidents, and proposed that the necessary condition for unstable failure of specimens is also a prerequisite for rock burst or coal burst [9,10]. In 1970, Salamon introduced the concept of local mine stiffness (LMS) and noted that if the LMS is "softer" than the post-peak stiffness of a coal pillar, the pillar would fail in an unstable and violent manner [11,23]. In the analysis of the The Galena Mine, Blake highlighted that the stiffness of the mine pillar exceeds that of the surrounding rock, a necessary condition for rock burst [12]. Jaiswal proposed a method for calculating the LMS based on numerical simulation results before and after coal pillar excavation [24]. Gu R. demonstrated through numerical simulation that as the working face advances, the LMS decreases, leading to an increased probability of instability of coal pillars and coal walls [25].

In addition to the vast amount of data documenting the occurrence of unstable failure in specimens tested on low-stiffness machines, there are also many results of experimental research that can empirically support the stiffness theory. Liu J.X., Li J.Q., and Dou L.M. individually conducted experiments on series-connected combined coal and rock samples, uniformly showed that a decrease in loading stiffness correlates with an increase in the bursting intensity of coal sample failure [26–28]. Furthermore, Gu J.C. et al. successfully reproduced ejective rock burst in indoor experiments by reducing the loading stiffness through the addition of series spring [29].

Zhang M.T. proposed that the the involvement of the surrounding rock in energy release is a necessary condition of coal burst, and deduced, based on the principle of minimum potential energy, that this prerequisite is equivalent to the LMS being smaller than the post-peak equivalent stiffness of the coal mass [14]. Tang C.A. [15], Pan Y.S. [16], and Wang S.Y. [17] derived, using the cusp-type catastrophe theory, that the instability failure or coal burst requires a stiffness ratio between the surrounding rock and the coal mass of less than 1. Although the theoretical basis of these studies differs, their conclusions align with the stiffness theory. These theoretical research findings have further enhanced the credibility of the stiffness theory.

While the stiffness theory has garnered significant experimental support and aligns with numerous theoretical research findings, it is not without its shortcomings. One of the notable drawbacks lies in its inability to reconcile with practical engineering experience. According to the stiffness theory, a decrease in the LMS increases the likelihood of system instability. However, in real-world engineering scenarios, coal seams often exhibit a higher propensity for coal burst occurrences under conditions of high-stiffness and hard roof or floor [3,30]. This contradiction with engineering experience poses a challenge to the widespread acceptance and recognition of the stiffness theory.

In this paper, several commonly overlooked aspects of stiffness theory are clarified and a qualitative risk evaluation formula for coal burst is presented. Furthermore, the uneven stiffness coal seam structure (USCS), which has the functions of pressure concentration and stiffness reduction, is proposed based on the stiffness theory and "three factors" mechanism. These two functions enable the USCS to address the contradiction between the stiffness theory and engineering practical experience to a certain extent, and rendering it a novel structural factor that is prone to coal burst, distinct from the existing factors within the "three factors" mechanism. The influence of key parameters of USCS on its ability to focus pressure, reduce stiffness, and increase the risk of coal burst is discussed through theoretical analysis and simple numerical simulations. Relevant conclusions provide new explanations for engineering phenomena such as time-delayed effects of some coal bursts, inefficient pressure relief in ultra thick coal seams, and "microseism deficiency" Before occurrence of certain coal bursts.

2. Details in Stiffness Theory

In 1970, Salamon put forth the conditions for specimen unstable failure through energy analysis [11]. It is mathematically given as:

$$k_{\mathrm{p}}/|\lambda_{\mathrm{b}}| < 1 \tag{1}$$

where k_{p} is the stiffness of the testing machine, λ_{b} is the average slope of the load-displacement curve of the specimen during the post-peak strain softening stage, and $|\lambda_{\mathrm{b}}|$ is referred to as the post-peak stiffness. The instability failure of the specimen on the flexible testing machine bears resemblance to coal burst. In both scenarios, pressure is exerted by the pressure provider, resulting in the failure of the pressure bearer while the pressure provider remains relatively intact. Both the specimen and coal mass serve as pressure bearers, with the relevant variables denoted by subscript b. Similarly, the testing machine and surrounding rock (the local mine composed of roof, coal, and floor strata around the coal mass) act as pressure providers, with the relevant variables indicated by subscript p. Therefore, Equation (1), initially depicting the necessary condition for specimen instability failure, can also be considered a prerequisite for coal burst, it can be referred to as the stiffness criterion, where $|\lambda_{\mathrm{b}}|$ denotes the post-peak stiffness of the coal mass that undergo failure after the peak, and k_{p} represents the local mine stiffness (LMS), which is the equivalent stiffness of the surrounding rock (pressure provider). According to the definition of LMS and the calculating method proposed by Jaiswal [11,23,24], The LMS of a coal pillar can be calculated with Equation (2).

$$k_{\mathrm{p}} = \frac{\Delta F_{\mathrm{p}}}{\Delta h} = \frac{f_1}{d_1 - d_2} \tag{2}$$

where f_1 is load suffered by the pillar, d_1 and d_2 are the distances between the roof and the floor before and after coal mass is mined, respectively. as shown in Figure 1.

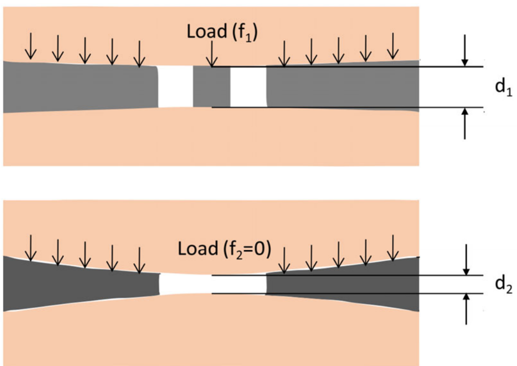

Figure 1. LMS calculation using numerical modeling [24].

By analyzing the stiffness theory, the following three details that were easily overlooked in previous research can be identified:

1. The stiffness criterion is a post-peak instability condition. So when discussing the stiffness criterion, it is already assumed that the coal mass satisfies the failure criterion. Therefore, the necessary conditions for coal burst according to the stiffness theory contain both the failure criterion and the stiffness criterion. The former determines whether the coal undergoes failure and enters the post-peak stage, providing the

basis for the latter. The latter determines whether the system instability occurs and is crucial in determining the burst intensity of failure.

2. The boundary between the specimen and testing machine is clear-cut, whereas determining the exact boundary between the coal mass and surrounding rock prior to the peak is diffcult. The determination of $|\lambda_b|$ laterally becomes more complex due to this factor. In this case, it might be wiser to initially evaluate the relative risk of coal bursts by utilizing Equation (3).

$$r_{CB} = r_F \times r_I \tag{3}$$

where r_{CB} is the probability of rock burst occurrence, known as the risk of coal burst; r_F is the probability of coal mass failure, known as the risk of failure; r_I is the probability that the system meeting the stiffness criterion and experiencing post-peak instability, known as the risk of instability. Higher values of dynamic and static loads, as well as lower coal strength and confining pressure, increase the likelihood of meeting the failure criterion, resulting in a higher r_F. While, lower values of k_p or higher values of $|\lambda_b|$ make it easier to satisfy the stiffness criterion and post-peak instability, leading a higher r_I.

3. Stiffness is a structural parameter rather than a material parameter. A flexible testing machine can be seen as a structure with a harder material but lower stiffness than the specimen. Hence, structures incorporating highly rigid materials (with high elastic modulus) while maintaining lower stiffness characteristics do exist. If such a structure situated within coal measure strata experiences a coal burst, it will conform to both the stiffness theory and engineering experience.

3. Uneven Stiffness Coal Seam Structure (USCS)

3.1. Structure Composition, Functions, and Typical Examples of USCS

Cook modified the flexible testing machine by adding a copper pipe parallel connection with the crossbeam to reduce its bending deformation and increase its stiffness, enabling the testing machine measure the post-peak curve of the rock for the first time [31,32]. If a special structure similar to a flexible testing machine exists within the coal measure strata, the key parts responsible for reducing the LMS through bending, similar to the flexible testing machine's crossbeam, would be the roof or the floor. To achieve bending in either the roof or the floor, it is necessary for varying compression deformations to occur at different positions along the coal seam, which implies that the normal stiffness of the coal seam is uneven. Hence, this unique structure within the coal measure strata can be termed as the Uneven Stiffness Coal seam Structure (USCS). USCS is composed of continuous roof and floor that sandwich coal seam with uneven stiffness distribution. The uneven distribution of stiffness is quantified using the Normal Stiffness Coefficient (NSC), which represents the normal stiffness per unit area and is measured in N/m^3. Within the USCS, sections of the coal seam with higher NSC values are identified as high stiffness zone (HSZ), whereas regions with lower NSC values are classified as low stiffness zone (LSZ). On the other hand, the Even Stiffness Coal Seam Structure (ESBS) represents the contrasting counterpart of USCS, comprising continuous roof and floor along with a coal seam exhibiting an even distribution of stiffness. Figure 2 provides a visual comparison between USCS and two types of ESCS.

The uneven distribution of normal stiffness enable USBS to have pressure concentration function which make the HSZ bears a higher static pressure under evenly distributed overlying loads. This function results in the coal mass of HSZ reaching the failure criterion more easily. Once the failure criterion is reached, the coal mass of HSZ would serves as a pressure bearer and undergoes failure, while the surrounding rock, including the roof, floor, and coal seam of LSZ in series, serves as a pressure provider and releases stored energy. Due to the overall stiffness of the series structure being lower than the stiffness of any constituent unit, the LMS of HSZ is in a state lower than the normal stiffness of LSZ. Therefore, the HSZ can exhibits lower LMS even when the roof and floor are hard, thus reconciling the contradiction between stiffness theory and engineering common sense. USCS exhibits both the pressure concentration function and the stiffness reduction function. The former enables stress to concentrate from the LSZ to the HSZ, thereby increasing the risk (r_F) of failure. The latter reduces the LMS of HSZ, making it easier to meet the stiffness criterion and leading to post-peak instability, thus elevating the risk (r_I) of instability. In contrast, ESBS lacks any pressure concentration or stiffness reduction function, regardless of the normal stiffness of the coal seam. Equation (3) supports the conclusion that the risk (r_{CB}) of coal burst in HSZ of USCS surpasses that in ESBS. Therefore, USCS is a structural factor prone to coal burst incidents.

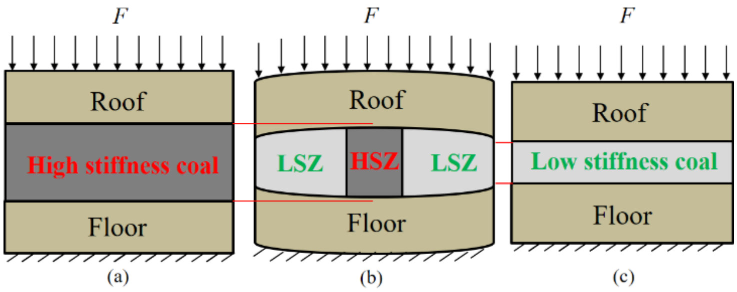

Figure 2. Comparison between USCS and two types of ESCS: (**a**) ESCS with high stiffness coal seam. (**b**) USCS with uneven stiffness coal seam. (**c**) ESCS with low stiffness coal seam.

In the case of a uniform rock stratum with an elastic modulus represented by E and a thickness denoted by H, Equation (4) can be employed to calculate the NSC.

$$K = k/S = E/H \tag{4}$$

Equation (4) states that altering the elastic modulus of coal or the thickness of the coal seam can both modify the NSC of the coal seam. Thinning the thickness of coal seam in certain areas or replacing certain sections of the local coal seam by rock with higher elastic modulus can both increase NSC, leading to the formation of USCS. For a compound coal seam with a total thickness of H, a coal elastic modulus of E_c, and the inclusion of strata with a thickness of h_r and an elastic modulus of E_r ($>E_c$), the normal stiffness coefficient of the composite coal seam, denoted as K_{c+r}, satisfies Equation (5).

$$K_{c+r} = \frac{E_c}{H-h_r} \cdot \frac{E_r}{h_r} / \left(\frac{E_c}{H-h_r} + \frac{E_r}{h_r} \right) = \frac{E_c}{H - h_r + h_r \cdot E_c/E_r} > \frac{E_c}{H} = K_c \tag{5}$$

According to Equation (5), when the overall thickness of the coal seam and the elastic modulus of the coal remain constant, the NSC (K_{c+r}) of a composite coal seam containing igneous rock or rock parting is higher than that of a pure coal seam. As a result, the magmatic intrusion areas or the bifurcation areas of coal seam will be categorized as HSZ of USCS. The USCS in Figure 2b, resulting from variations in elastic modulus of coal is known as material USCS, while the USCS arising from changes in coal seam thickness or the ratio of coal rock thickness is referred to as thickness USCS.

Coal seam thinning zones, bifurcation areas, magmatic intrusion areas are all areas with high incidence of coal burst. In Tianchi Coal Mine in Sichuan, China, about half of the 28 major coal burst accidents happened in areas where the coal seam thickness underwent sudden changes, like floor protrusion zones, zones with sharp changes in coal seam dip angles, coal seam thinning zones, and strata pinch-out zones [3]. Notable coal burst incidents, such as the "7.29" event on the 1305 working face of Zhaolou Coal Mine of Yankuang Group in 2015 and the "10.20" major coal burst disaster on the 1303 working face of Shandong Longyun Coal Mine in 2018, occurred near coal seam bifurcation zones [33]. Similarly, coal mines like Pingzhuang Gushan, Huaibei Haizi, and Shandong Liangbaosi have all experienced coal burst accidents near magmatic intrusion areas [34]. Despite the varying locations depicted in Figure 3, the common feature among these coal burst locations is exhibit higher normal stiffness than the surrounding regions. To gain a unified understanding and implement targeted prevention and control measures based on their shared characteristics, these areas can be classified as HSZs of USCS.

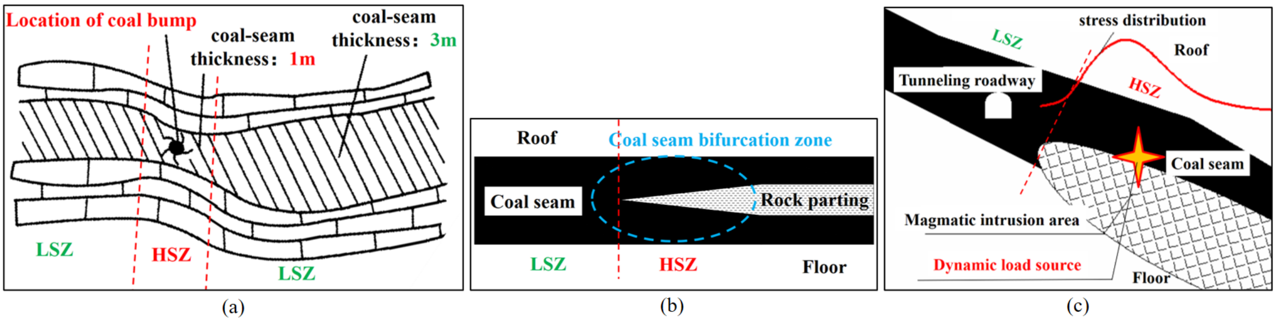

Figure 3. Three kinds of typical USCS in coal measure strata: (**a**) Coal seam thinning zone (a certain coal burst accident in Tianchi Coal Mine, Sichuan) [3]. (**b**) Coal seam bifurcation area. (**c**) Magmatic intrusion area (2015 "8.5" coal burst accident in a coal mine in Inner Mongolia) [34].

3.2. Analysis of Pressure Concentration Function of USCS

Many scholars attribute the occurrence of coal burst to stress concentration and link the cause of stress concentration to tectonic stress without delving into the topic extensively. However, the natural USCS represents a range of tectonic structures. Under conditions of uniform distribution of overlying loads, stress tends to concentrate from LSZ to HSZ, particularly at the boundary between HSZ and LSZ (HSZ-LSZ boundary).

Figure 4 illustrates the simplified analysis conducted to study the stress distribution in an uneven stiffness coal seam under a uniformly distributed load. The approach involves fixing the floor and considering only the deformation of the coal seam and roof. The focus is on examining the normal deformation and normal stress distribution in the coal seam under three different scenarios.

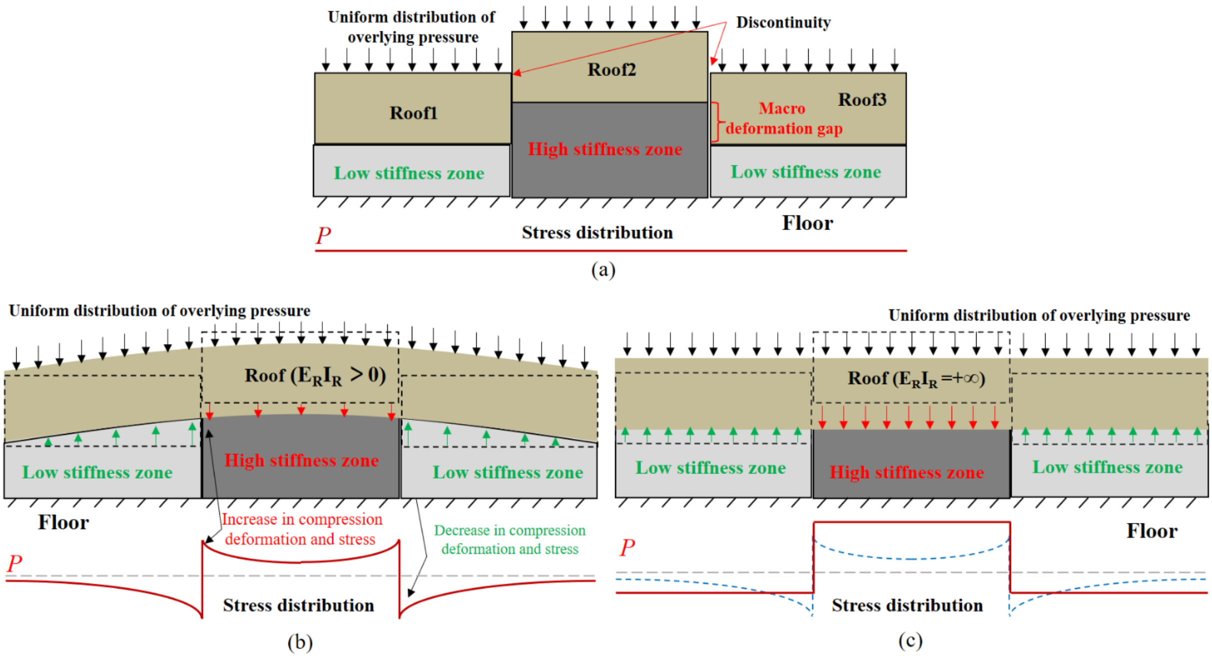

Figure 4. Stress distribution and deformation of uneven stiffness coal seam under three kinds of roof: (**a**) discontinuous roof and coal seam. (**b**) continuous elastic roof and coal seam. (**c**) rigid roof and continuous elastic coal seam.

In the first scenario, if the roof and coal seam exhibit extreme flexibility (with a bending stiffness of 0) or if there are discontinuities at the HSZ-LSZ boundaries, the normal stress in each area of the coal seam will be uniformly distributed and denoted as P. However, a macro deformation gap will be present between the HSZ and LSZ, as depicted in Figure 4a.

Moving to the second scenario, when the roof is continuous and possesses a finite bending stiffness greater than 0, it will bend to eliminate the macroscopic deformation gap and maintain a continuous coordination of deformation. This bending action leads to increased compression deformation in HSZ, particularly at its boundary, and reduced compression deformation in LSZ, especially at its boundary. As a result, the normal stress in the coal seam will be greater than P in HSZ and less than P in LSZ, as shown in Figure 4b. Considering the premise of maintaining the bending stiffness of the roof, the greater the difference in normal stiffness between the HSZ and LSZ, the more significant the bending deflection of the roof, leading to a higher concentration of normal stress in HSZ.

The third scenario involves a continuous roof with infinite bending stiffness, thereby preventing any bending from occurring. Consequently, the deformation in both the HSZ and LSZ will be forced to be consistent, as depicted in Figure 4c. In this case, the normal stress σ_{yH}' in HSZ and σ_{yL}' in LSZ will satisfy Equation (6).

$$\begin{cases} \sigma_{y\mathrm{H}}' S_{\mathrm{H}} + \sigma_{y\mathrm{L}}' S_{\mathrm{L}} = P(S_{\mathrm{H}} + S_{\mathrm{L}}) \\ \sigma_{y\mathrm{H}}' S_{\mathrm{H}} / k_{\mathrm{H}} = \sigma_{y\mathrm{L}}' S_{\mathrm{L}} / k_{\mathrm{L}} = \sigma_{y\mathrm{H}}' / K_{\mathrm{H}} = \sigma_{y\mathrm{L}}' / K_{\mathrm{L}} \end{cases} \tag{6}$$

where, K_{H} and S_{H} is the NSC and area of the HSZ, respectively; and K_{L} and S_{L} is the NSC and area of LSZ, respectively. The solution of Equation (6) can be writed as follows:

$$\begin{cases} \sigma_{y\mathrm{H}}' = \frac{P(S_{\mathrm{H}}/S_{\mathrm{L}}+1)}{(S_{\mathrm{H}}/S_{\mathrm{L}}+K_{\mathrm{L}}/K_{\mathrm{H}})} = P + \frac{P(1-K_{\mathrm{L}}/K_{\mathrm{H}})}{(S_{\mathrm{H}}/S_{\mathrm{L}}+K_{\mathrm{L}}/K_{\mathrm{H}})} \\ \sigma_{y\mathrm{L}}' = \frac{P(S_{\mathrm{L}}/S_{\mathrm{H}}+1)}{(S_{\mathrm{L}}/S_{\mathrm{H}}+K_{\mathrm{H}}/K_{\mathrm{L}})} = P + \frac{P(1-K_{\mathrm{H}}/K_{\mathrm{L}})}{(S_{\mathrm{L}}/S_{\mathrm{H}}+K_{\mathrm{H}}/K_{\mathrm{L}})} \end{cases} \tag{7}$$

Upon observing Equation (7), it becomes evident that the ratio $K_{\mathrm{H}}/K_{\mathrm{L}}$ exhibits a positive correlation with σ_{yH}' and a negative correlation with σ_{yL}'. Given that $K_{\mathrm{L}}/K_{\mathrm{H}}$ is less than 1 (indicating that the NSC of the coal seam in HSZ must surpass that of the LSZ), it follows that σ_{yH}' must exceed P and displays a negative correlation with $S_{\mathrm{H}}/S_{\mathrm{L}}$, or equivalently, a positive correlation with $S_{\mathrm{L}}/S_{\mathrm{H}}$. Similarly, $K_{\mathrm{H}}/K_{\mathrm{L}}$ is greater than 1, and σ_{yL}' must be less than P and also exhibits a positive correlation with $S_{\mathrm{L}}/S_{\mathrm{H}}$.

The true normal stress (σ_{yH}) in HSZ falls between the values of P and σ_{yH}'. Moreover, as the bending stiffness of the roof increases, σ_{yH} approaches σ_{yH}' more closely, establishing a positive correlation between σ_{yH} and the roof's bending stiffness. Typically, the roof is simplified as a rectangular cross-section beam, with the bending stiffness being the product of the elastic modulus (E_{R}) of the roof and the inertia moment (I_{R}) of the roof section. It is worth noting that the I_{R} is positively correlated with the roof's thickness (H_{R}). Considering that σ_{yH}' represents the limit of σ_{yH}, it can be inferred that σ_{yH} is similar to σ_{yH}' and shows a positive correlation with E_{R}, H_{R}, $K_{\mathrm{H}}/K_{\mathrm{L}}$ and $S_{\mathrm{L}}/S_{\mathrm{H}}$. Similarly, it can be deduced that σ_{yL} exhibits a negative correlation with E_{R}, H_{R}, and $K_{\mathrm{H}}/K_{\mathrm{L}}$ but a positive correlation with $S_{\mathrm{L}}/S_{\mathrm{H}}$.

It is evident that the pressure concentration function of USCS induces stress concentration under a uniform overlying pressure. The higher elastic modulus (E_{R}) or larger thickness (H_{R}) of roof make it harder to bend, leading more concentrated stress states appear in HSZ. Additionally, the discrepancy in stiffness ($K_{\mathrm{H}}/K_{\mathrm{L}}$) and area ($S_{\mathrm{L}}/S_{\mathrm{H}}$) between HSZ and LSZ leads to an increased load per unit area in HSZ, exacerbating stress concentration. Besides superimposing mining stress or external dynamic loads, enhancing the value of $E_{\mathrm{R}}H_{\mathrm{R}}K_{\mathrm{H}}S_{\mathrm{L}}/K_{\mathrm{L}}S_{\mathrm{H}}$ in the USCS can also further improve σ_{yH}, consequently enabling the coal mass in HSZ to approach or reach the failure criterion.

3.3. Analysis of Stiffness Reduction Function of USCS

A simplified model of the coal mass-surrounding rock system during the failure process, focusing on the roof deformation while neglecting the influence of gravity and floor deformation, is depicted in Figure 5. When the coal mass reaches its peak pressure, both the internal force (F_b) of the coal mass and the internal force (F_p) of roof experience the maximum load, F_{max}. Post-peak, F_b decreases due to the strain softening of the coal mass, while F_p decreases due to roof deformation recovery.

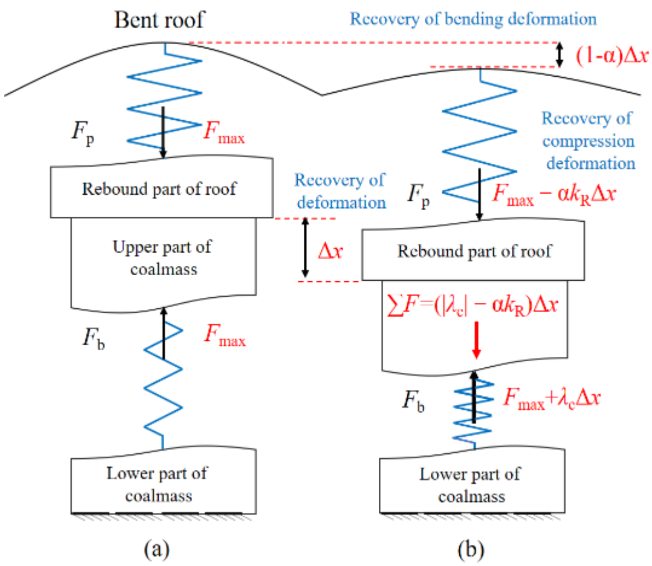

Figure 5. Simplified model of the coal mass-surrounding rock system with bent roof: (**a**) System at peak: two force equilibrium; (**b**) Post peak system: recovery of bending deformation.

During the failure process, the overall amount of roof deformation recovery is denoted by Δx. In the case of ESCS, the roof has no bending deformation under uniform overlying loads. At this stage, the amount of recovery is Δx for compression deformation, so the local mine stiffness (k_p) is equal to the normal stiffness (k_R) of the roof, which can be computed using Equation (8).

$$k_p = k_R = E_R S_R / H_R \tag{8}$$

In contrast, when USCS sustains uniform overlying loads, both compression deformation and bending deformation of the roof and floors recover. The recovery amount of compression deformation is $\alpha \Delta x$, where α is the stiffness reduction coefficient of the USCS and is greater than 0 but less than 1. Consequently, the recovery amount of roof bending deformation is (1-α)Δx. The reduction in internal force (ΔF_p) of the pressure provider is solely proportional to the recovery amount of compression deformation, with $\alpha K_R \Delta x$ representing the decrease in internal force. So the LMS (k_p) is determined using Equation (9) and must be less than k_R.

$$k_p = \Delta F_p / \Delta x = k_R \alpha \Delta x / \Delta x = \alpha k_R = \alpha E_R S_R / H_R \tag{9}$$

Equation (9) illustrates that bending of the roof can reduce its internal force reduction under the same amount of deformation recovery after the peak, leading to a decrease in the LMS. Through a stiffness theory analysis, it becomes apparent that a lower LMS yields greater compliance with stiffness criterion, thereby elevating the risk of instability (r_I). Thus, when compared to the ESCS operating under identical conditions, the USCS exhibits a higher r_I owing to its stiffness reduction function.

Figure 6 illustrates a trisection model of the USCS, where the roof is simplified as a flexible rectangular cross-section beam and the HSZ or LSZ is represented as hard springs

(k_{H}) or soft springs (k_{L}). Assuming that the discrepancy between the internal force F_{L} representing the LSZ and the average load is ΔF, Equation (10) can be deduced.

$$\begin{cases} y_{\mathrm{L}} = F_{\mathrm{L}}/k_{\mathrm{L}} = (F/3 - \Delta F)/k_{\mathrm{L}} \\ y_{\mathrm{H}} = F_{\mathrm{H}}/k_{\mathrm{H}} = (F/3 + 2\Delta F)/k_{\mathrm{H}} \\ w = y_{\mathrm{L}} - y_{\mathrm{H}} = \Delta F l^3/24E_{\mathrm{R}}I_{\mathrm{R}} \end{cases} \tag{10}$$

where, F_{H} and F_{L} represent the internal force of the spring in HSZ and LSZs, y_{H} and y_{L} represent the compression deformation of the hard and soft springs, w is the bending deflection of the roof, and l is the lateral span of the structure. Equation (11) can be inferred from Equation (10).

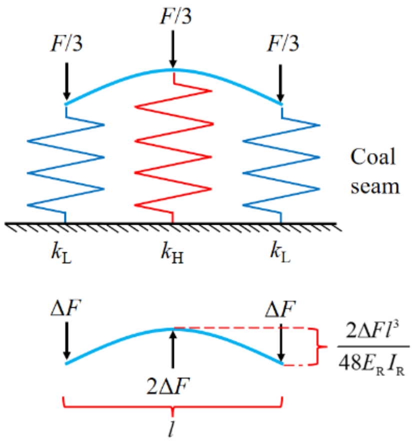

Figure 6. The trisection model of the USCS.

$$\begin{cases} \Delta F = \frac{(k_{\mathrm{H}}-k_{\mathrm{L}})F/3}{2k_{\mathrm{L}}+k_{\mathrm{H}}+(k_{\mathrm{L}}k_{\mathrm{H}})l^3/24E_{\mathrm{R}}I_{\mathrm{R}}} = \frac{(1-1/(k_{\mathrm{H}}/k_{\mathrm{L}}))\cdot F/3}{1+2/(k_{\mathrm{H}}/k_{\mathrm{L}})+k_{\mathrm{L}}l^3/24E_{\mathrm{R}}I_{\mathrm{R}}} \\ w = \frac{\Delta F l^3}{24E_{\mathrm{R}}I_{\mathrm{R}}} = \frac{F/3\cdot(1-1/(k_{\mathrm{H}}/k_{\mathrm{L}}))l^3}{(1+2/(k_{\mathrm{H}}/k_{\mathrm{L}})+k_{\mathrm{L}}l^3/24E_{\mathrm{R}}I_{\mathrm{R}})\cdot 24E_{\mathrm{R}}I_{\mathrm{R}}} = \frac{F/3\cdot(1-1/(k_{\mathrm{H}}/k_{\mathrm{L}}))l^3}{(24E_{\mathrm{R}}I_{\mathrm{R}}+48E_{\mathrm{R}}I_{\mathrm{R}}/(k_{\mathrm{H}}/k_{\mathrm{L}})+k_{\mathrm{L}}l^3)} \end{cases} \tag{11}$$

Given that the roof's rotational inertia (I_{R}) is positively correlated with its thickness (H_{R}), it becomes evident from Equation (11) that both $E_{\mathrm{R}}H_{\mathrm{R}}$ and $K_{\mathrm{H}}/K_{\mathrm{L}}$ exhibit positive correlations with the value of ΔF. This observation reinforces the previously discussed findings regarding the impact of cohesive forces, as ΔF serves as an indicator of stress concentration in HSZ. It should be noted that w demonstrates a positive relationship with $K_{\mathrm{H}}/K_{\mathrm{L}}$, but a negative relationship with $E_{\mathrm{R}}H_{\mathrm{R}}$. By incorporating the stiffness definition and combining Equations (9) and (11), the stiffness k_{p} of the surrounding rock can be determined using Equation (12) within the trisection model of USCS.

$$k_{\mathrm{p}} = \frac{\Delta F_{\mathrm{p}}}{\Delta x} = \frac{F_{\mathrm{H}}}{w_{\mathrm{H}} + F_{\mathrm{H}}/k_{\mathrm{R}}} = \frac{1}{\Delta F l^3/((F/3+2\Delta F)24E_{\mathrm{R}}I_{\mathrm{R}}) + 1/k_{\mathrm{R}}} = \frac{1}{\left(l^3/\left(\frac{24E_{\mathrm{R}}I_{\mathrm{R}}+48E_{\mathrm{R}}I_{\mathrm{R}}/(k_{\mathrm{H}}/k_{\mathrm{L}})+k_{\mathrm{L}}}{(1-1/(k_{\mathrm{H}}/k_{\mathrm{L}}))} + 48E_{\mathrm{R}}I_{\mathrm{R}}\right) + \frac{H_{\mathrm{R}}}{E_{\mathrm{R}}l}\right)} \tag{12}$$

The stiffness ratio $k_{\mathrm{H}}/k_{\mathrm{L}}$ of the coal seam is equal to the NSC ratio $K_{\mathrm{H}}/K_{\mathrm{L}}$. Equation (12) indicates that the LMS (k_{p}) has a negative correlation with the NSC ratio $K_{\mathrm{H}}/K_{\mathrm{L}}$, and a positive correlation with the elastic modulus of the roof (E_{R}). In an ESCS, the $K_{\mathrm{H}}/K_{\mathrm{L}} = 1$, $w = 0$, so the k_{p} is equivalent to the stiffness (k_{R}) of the roof. On the other hand, in an USCS, the NSC ratio $K_{\mathrm{H}}/K_{\mathrm{L}}$ is greater than 1, resulting in a smaller k_{p} compared to k_{R}. This explains why the USCS exhibits a stiffness reduction function, while the ESCS does not. As the NSC ratio $K_{\mathrm{H}}/K_{\mathrm{L}}$ increases, the LMS decreases, making it easier to meet the stiffness criterion, leads to higher risk of instability (r_{I}) and coal burst (r_{CB}).

4. Simple Numerical Simulation of Uneven Stiffness Coal Seam Structure (USCS)

In previous analysis, it was found that the six key parameters of USCS positively or negatively affect the pressure concentration and stiffness reduction functions of USCS. To validate the previous analytical conclusions and examine the influence of various parameters of USCS on its two specific functions, 6 groups of 14 simplified 2D models using COMSOL 5.2 software was constructed. These models were created based on the controlled variables method, aiming to simulate different responses of the USCS under same working conditions but with varying parameters. To simplify calculations, no failure criteria and floor were established. The bottom of the coal seam restricts vertical displacement, while the top of the roof sustains an evenly distributed pressure of 15 MPa without any constraints on deformation. The the left and right boundaries of the roof and coal seam constrain the lateral displacement. The model's dimensions are 40 m long and 11–15 m high, with a 6 m thick coal seam, a 5–9 m thick roof rock stratum, and a coal rock stratum dip angle of 0°. The mesh division uses extreme fine with triangular elements and unit sizes ranging from 8×10^{-4} m to 0.4 m, resulting in 7082 to 9510 elements. The coal seam of models includes a HSZ and two LSZ with clear boundaries formed by the hard coal in the middle and the soft coal on both sides. The Poisson's ratio for the roof is set to 0.2, while the hard coal and soft coal have Poisson's ratios of 0.22 and 0.3, respectively. Detailed information regarding the model parameters can be found in Table 1. The 14 models were categorized into 6 groups based on different control variables (S_H, E_R, E_H, E_L, H_R, S_R or S_L). Model 1 served as a common member for each group, with the other models derived by modifying the values of the control variables in this group. Furthermore, modifying E_H and E_L is analogous to altering K_H and K_L, adjusting S_R when S_H remains unchanged would effectively modify S_L. The stress distribution and deformation of the models were computed, as depicted in Figure 7.

Table 1. Model parameters of 14 uneven stiffness coal seam structures.

Model	Width of Roof S_R/m	Thickness of Roof H_R/m	Young's Modulus of Roof E_R/GPa	Young's Modulus of Hard Coal in HSZ E_H/GPa	Young's Modulus of Soft Coal in LSZ E_L/GPa	Width of HSZ S_H/m	Width of LSZ (One Side) S_L/m
1	*40*	*5*	*20*	*5*	*2*	4	18
2	40	5	20	5	2	10	15
3	40	5	20	5	2	20	10
4	40	5	*15*	5	2	4	18
5	40	5	*10*	5	2	4	18
6	40	5	20	*4*	2	4	18
7	40	5	20	*3*	2	4	18
8	40	5	20	5	*1*	4	18
9	40	5	20	5	1×10^{-10}	4	18
10	40	5	20	5	*0*	4	*No Coal (goaf)*
11	40	*7*	20	5	2	4	18
12	40	*9*	20	5	2	4	18
13	*20*	5	20	5	2	4	*8*
14	*12*	5	20	5	2	4	*4*

By examining Figure 7, it is evident that:

(1) The normal stress and the Mises stress in HSZ demonstrate notably higher values compared to those in LSZ, providing evidence for the pressure concentration function of USCS. Furthermore, the roof displays bending deformation with its axis of symmetry aligned with the middle axis of the HSZ, substantiating the stiffness reduction function of USCS.

(2) At the HSZ-LSZ boundary, significant stress concentrations are present, particularly at the shoulders of the HSZ. These areas are prone to crack development, and the NSC varies as the cracks progress, resulting in a transitional zone where NSC undergoes continuous changes. This aids in reducing stress concentration at the boundary,

similar to decreasing the area (S_H) of the HSZ (The width of a two-dimensional model can represent the area in three-dimensional reality). Consequently, the actual stress distribution differs from the results of a simple simulation. For instance, regions of high stress shift towards the middle, moving away from the boundary of the HSZ. Nevertheless, this does not impact the overall pattern of stress concentration towards the HSZ and roof bending.

(3) Noteworthy discrepancies in stress distribution and roof deformation arise among different models within the same group. This indicates that the six parameters of USCS can influence pressure concentration and stiffness reduction functions.

The variations in normal stress (σ_y), roof compression deformation (u_yR), and roof bending deflection (w_R) along the horizontal axis of different USCS models in six groups are determined through simulation calculations, as depicted in Figure 8. In the figure, the σ_y represents the normal stress values at the nodes located on the median line of the coal seam (with a vertical coordinate of 3 m). The u_yR is calculated as the disparity between the normal displacement values of nodes located on the lower boundary and their corresponding nodes on the upper boundary of the roof. Moreover, the w_R is obtained by subtracting the minimum average normal displacement value from the mean normal displacement values calculated for the upper and lower boundary nodes of the roof. So the w_R on both sides of the roof is determined to be 0.

Based on Figure 8, the following observations can be made:

(1) The HSZ exhibits higher normal stress, compression deformation, and bending deflection compared to the LSZ in all models, confirming that the USCSs serves the dual functions of pressure concentration and stiffness reduction.

(2) In cases where the ratio of $S_\mathrm{L}/S_\mathrm{H}$ remains constant (group 2 to 5), models with higher normal stress in HSZ (σ_yH) exhibit lower normal stress in LSZ (σ_yL) compared to other models within the same group. This indicates that the increase in σ_yH is attributed to the HSZ bearing a larger portion of the load that should have been borne by the LSZ, thus causing a reverse change in σ_yH and σ_yL. However, if the ratio of $S_\mathrm{L}/S_\mathrm{H}$ changes (group 1 and 6), σ_yH and σ_yL decrease simultaneously with the decrease in $S_\mathrm{L}/S_\mathrm{H}$, demonstrating a consistent trend. This validates the conclusion derived from Equation (7) that both σ_yH and σ_yL are positively correlated with $S_\mathrm{L}/S_\mathrm{H}$.

(3) The variation gradient of NSC between the two points situated in HSZ and LSZ is positively correlated with the magnitude of the difference in normal stress. In other words, the variation in stress induced by the USCS is positively correlated with gradient of NSC between HSZ and LSZ. Reducing the gradient of NSC can alleviate stress concentration in HSZ, while increasing the variation gradient of NSC can exacerbate it.

Table 2 presents the calculated average normal stress concentration factor ($\overline{f}_\mathrm{scH}$), average stiffness reduction coefficient ($\overline{\alpha}$), and average normal stiffness coefficient ($\overline{K}_\mathrm{pH}$) in HSZ for different models based on the simulation results. These coefficients provide an overview of the HSZ and can be estimated using Equation (13).

$$\begin{cases} f_\mathrm{scH} = \overline{\sigma}_\mathrm{yH}/P \\ \overline{K}_\mathrm{pH} = \overline{\alpha} K_\mathrm{R} = \frac{\overline{u}_\mathrm{yRH}}{\overline{U}_\mathrm{yRH}} \cdot \frac{E_\mathrm{R}}{H_\mathrm{R}} = \frac{\overline{u}_\mathrm{yRH}}{\overline{u}_\mathrm{yRH} + \overline{w}_\mathrm{RH}} \cdot \frac{E_\mathrm{R}}{H_\mathrm{R}} \end{cases} \quad (13)$$

where, $\overline{\sigma}_\mathrm{yH}$ is the average normal stress value in HSZ; P is the overlying pressure, set to 15 MPa in the simulation; And $\overline{u}_\mathrm{yRH}$ and $\overline{w}_\mathrm{RH}$ are the average value of compression deformation and bending deflection of the roof in HSZ, respectively.

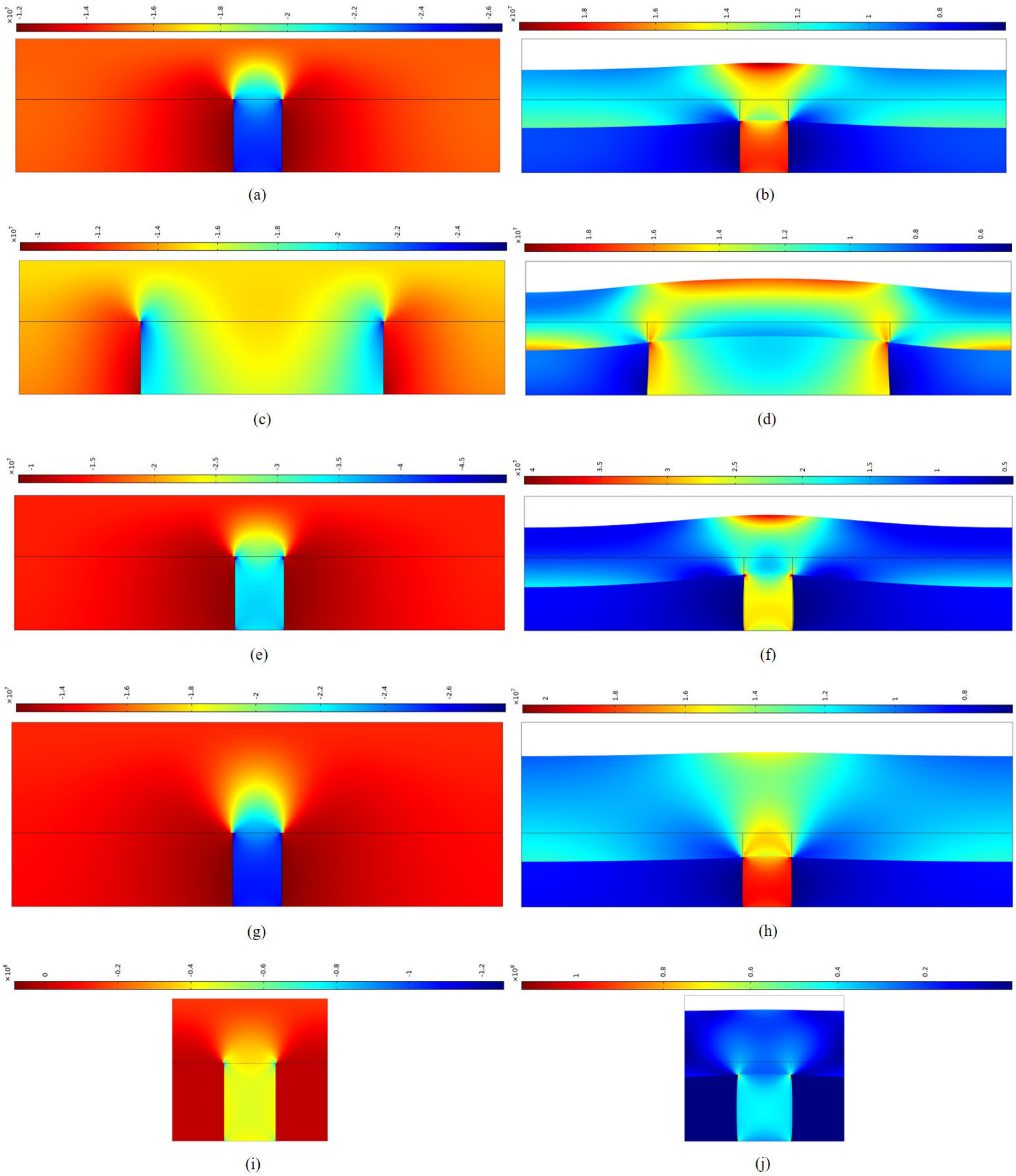

Figure 7. Simulation results of different USCS models (stress unit: Pa): (**a**) Normal stress cloud map of model 1 (common member); (**b**) Deformation and the Mises stress cloud map of model 1; (**c**) Normal stress cloud map of model 3 (S_H = 20 m); (**d**) Deformation and the Mises stress cloud map of model 3; (**e**) Normal stress cloud map of model 8 (E_L = 1 GPa); (**f**) Deformation and the Mises stress cloud map of model 8; (**g**) Normal stress cloud map of model 12 (H_R = 9 m); (**h**) Deformation and the Mises stress cloud map of model 12; (**i**) Normal stress cloud map of model 14 (S_R = 12 m); (**j**) Deformation and the Mises stress cloud map of model 14.

Analyzing the information provided in Table 2 reveals the following findings:

(1) Across all models of USCS, it is evident that the stress concentration factor of the HSZ (f_{scH}) consistently exceeds 1. Additionally, the LMS in HSZ (K_{pH}) remains lower than the stiffness of the roof (K_{R}). These findings indicate that USCS exhibits the dual characteristics of pressure concentration and stiffness reduction functions.

(2) The $\overline{\sigma}_{\mathbf{yH}}$ (average normal stress in HSZ) positively correlates with E_{R}, H_{R}, K_{H}, and S_{L}, but negatively correlates with K_{L} and S_{H}; The $\overline{K}_{\mathrm{pH}}$ (average LMS per unit area in HSZ) negatively correlates with H_{R}, K_{H}, S_{L}, and S_{H}, but positively correlates with E_{R} and K_{L}.

(3) An increase in the E_{R} leads to a relatively smaller growth in K_{pH}. When switch Model 1 to Model 5, where E_{R} increases from 10 GPa to 20 GPa, the stiffness of the roof (K_{R}) shows a 100% increase. In contrast, the relative increase in K_{pH} is only 41.7%. The reduction in the value of α helps partially offset the influence of roof hardening on the stiffness of the surrounding rock.

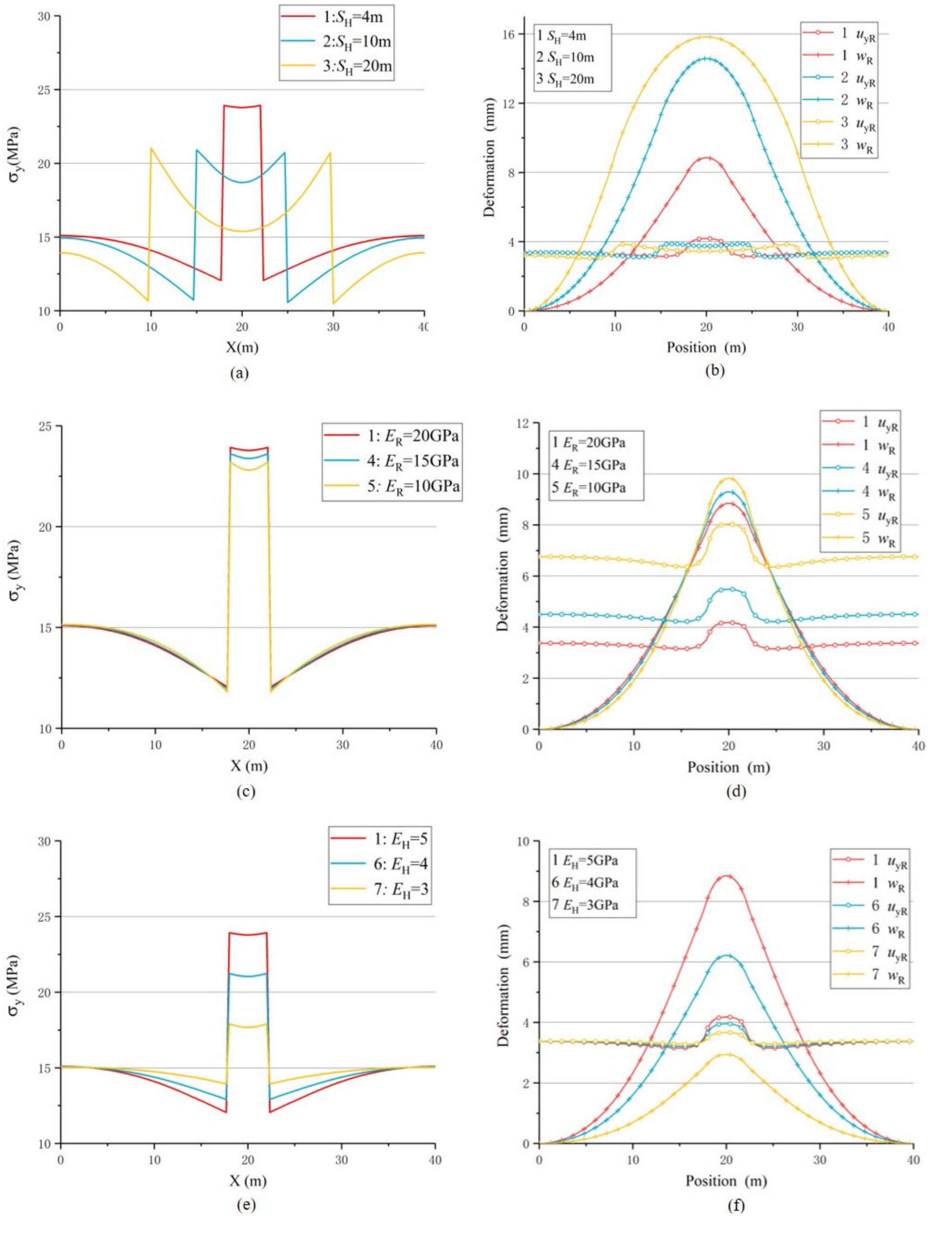

Figure 8. *Cont.*

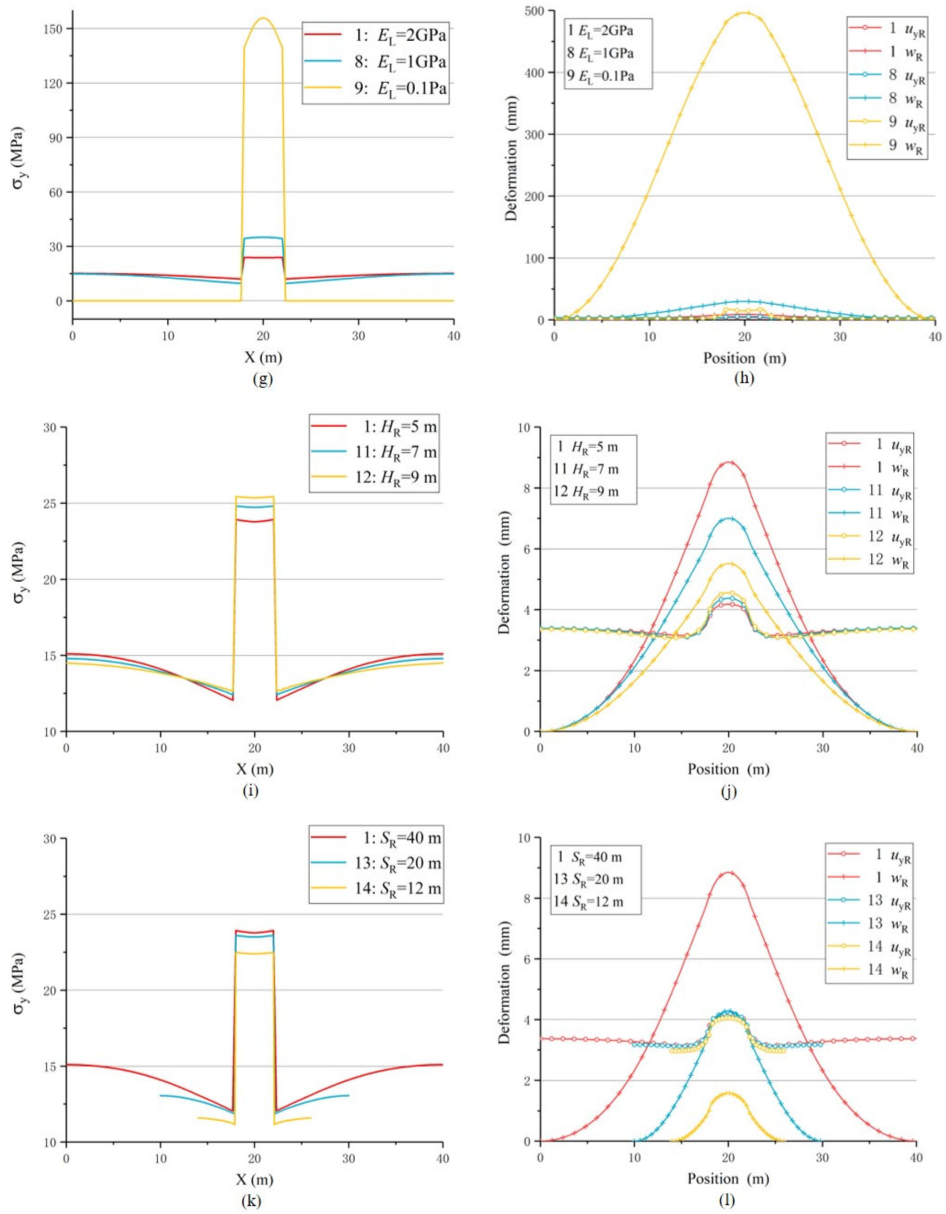

Figure 8. Variation curves of σ_y, u_{yR} and w_R of USCS models in six groups: (**a**) Curves of σ_y of models with different S_H; (**b**) Curves of u_{yR} and w_R of models with different S_H; (**c**) Curves of σ_y of models with different E_R; (**d**) Curves of u_{yR} and w_R of models with different E_R; (**e**) Curves of σ_y of models with different $K_H(E_H)$; (**f**) Curves of u_{yR} and w_R of models with different K_H; (**g**) Curves of σ_y of models with different $K_L(E_L)$; (**h**) Curves of u_{yR} and w_R of models with different K_L; (**i**) Curves of σ_y of models with different H_R; (**j**) Curves of u_{yR} and w_R of models with different H_R; (**k**) Curves of σ_y of models with different $S_L(S_R)$; (**l**) Curves of u_{yR} and w_R of models with different S_L.

In the mechanism analysis and simplified simulation, six key parameters of USCS are involved, namely, thickness (H_R) of roof, elastic modulus (E_R) of roof, NSC of HSZ (K_H), NSC of LSZ (K_L), area (S_H) of HSZ, and area (S_L) of LSZ. These parameters can have either positive or negative effects on the pressure concentration function and stiffness reduction function of the USCS, thereby influencing the risk of failure, instability, and coal burst in HSZ. By considering mining, fracturing, blasting, drilling, and slot cutting as a reduction in stiffness of coal seam, and considering support and backfilling as an increase in stiffness of coal seam, and treating goaf or roadway as an LSZ of the artificial USCS, it is possible to reconsider past engineering experience and summarize the impact of these six key parameters on indicators related to impact risk. Table 3 presents the correlations between the six key parameters and risk indicators of coal burst, which are derived from the analysis results, simulation results, and engineering experience.

Table 2. Average value of calculation results in HSZs of 14 USCS models.

No.	Controlled Variable	Controlled Variable Value	Normal Stress $\overline{\sigma}_{yH}$/MPa	Stress Concentration Factor $\bar{f}_{scH}$	Compression Deformation $\overline{u}_{yRH}$/mm	Bending Deflection $\overline{w}_{RH}$/mm	Total Deformation $\overline{U}_{yRH}$/mm	NSC of RoofK_R/N·mm^{-3}	$\overline{\alpha}$	NSC of Pressure Provider $\overline{K}_{pH}$/N·mm^{-3}
1	S_H/m	4	23.837	1.589	4.065	8.569	12.635	4.000	0.322	1.287
2		10	19.576	1.305	3.798	13.471	17.269	4.000	0.220	0.880
3		20	17.442	1.163	3.602	13.638	17.241	4.000	0.209	0.836
1	E_R/GPa	20	23.847	1.589	4.065	8.569	12.635	4.000	0.322	1.287
4		15	23.469	1.564	5.346	8.978	14.324	3.000	0.373	1.120
5		10	22.955	1.530	7.861	9.453	17.314	2.000	0.454	0.908
1	E_H/Gpa (K_H)	5	23.837	1.589	4.065	8.569	12.635	4.000	0.322	1.287
6		4	21.110	1.407	3.862	6.007	9.869	4.000	0.391	1.565
7		3	17.759	1.184	3.608	2.830	6.438	4.000	0.564	2.242
1	E_L/GPa (K_L)	2	23.837	1.589	4.065	8.569	12.635	4.000	0.322	1.287
8		1	34.829	2.322	4.996	29.159	34.155	4.000	0.146	0.585
9		1×10^{-10}	149.758	9.984	15.640	490.043	505.683	4.000	0.031	0.124
10		0	149.758	9.984	15.640	490.043	505.683	4.000	0.031	0.124
1	H_R/m	5	23.837	1.589	4.065	8.569	12.635	4.000	0.322	1.287
11		7	24.762	1.651	4.220	6.785	11.005	2.857	0.383	1.096
12		9	25.385	1.692	4.379	6.003	10.382	2.222	0.422	0.937
1	S_R/m (S_L/m)	40 (*18*)	23.837	1.589	4.065	8.569	12.635	4.000	0.322	1.287
13		20 (*8*)	23.541	1.569	4.093	4.059	8.152	4.000	0.502	2.008
14		12 (*4*)	22.427	1.495	3.961	1.431	5.393	4.000	0.735	2.938

Table 3. Correlation between the six key parameters of USCS and coal burst risk of high stiffness zone.

Key Parameters	Mechanical Analysis					Numerical Simulation					Engineering Experience		Corresponding Available Ways of Coal Burst Prevention
	f_{scH}	r_F	k_{pH}	r_I	r_{CB}	f_{scH}	r_F	K_{pH}	r_I	r_{CB}	f_{scH}	r_{CB}	
$\boldsymbol{S_H}$	-	-				-	-	-	+		-	**-**	Avoiding a decrease in $\boldsymbol{S_H}$: Avoid mining isolated working faces
$\boldsymbol{E_R}$	+	+	+	-		+	+	+	-		+	**+**	Reduce $\boldsymbol{E_R}$ of continuous composite roof: Carried out roof cutting measures in rock stratum with higher E_R.
$\boldsymbol{E_H}$ ($\boldsymbol{K_H}$)	+	+	-	+	**+**	+	+	-	+	**+**	+	**+**	Reduce $\boldsymbol{K_H}$: coal seam slotting or blasting, large diameter pressure release drilling, water injection softening, high pressure water jet cutting
$\boldsymbol{E_L}$ ($\boldsymbol{K_L}$)	-	-	+	-	**-**	-	-	+	-	**-**	-	**-**	Increase $\boldsymbol{K_L}$: hydraulic support, single prop, anchor bolts and cables, grouting, goaf filling
$\boldsymbol{H_R}$	+	+				+	+	-	+	**+**	+	**+**	Reduce $\boldsymbol{H_R}$ of continuous composite roof: Carried out roof cutting measures in rock stratum with higher H_R.
$\boldsymbol{S_L}$ ($\boldsymbol{S_R}$)	+	+				+	+	-	+	**+**	+	**+**	Cutting roof or floor to reduce the $\boldsymbol{S_R}$ ($\boldsymbol{S_L}$): directional hydraulic fracturing, deep hole blasting

+: Positive Correlation, -: Negative Correlation, leave a blank space: Uncertain Correlation.

From Table 3, it can be seen that:

(1) When E_R, H_R, K_H, and S_L increase, or K_L and S_H decrease, the pressure concentration function of the USCS becomes stronger, resulting in a higher concentration of stress and an increased risk (r_F) of failure in HSZ. When H_R, K_H, S_L, and S_H increase, or E_R and K_L decrease, the stiffness reduction function of the USCS becomes stronger, leading to lower LMS and an increased risk (r_I) of instability in HSZ.

(2) The analysis results and simulation results are in agreement with engineering experience in many cases, affirming the suitability of utilizing uneven stiffness coal seam structure for investigating coal burst phenomena.

(3) Reduce K_H, S_L (S_R), or increase K_L of USCS can simultaneously decrease the r_F and r_I, thus decrease r_{CB}. The majority of existing engineering measures for coal

burst preventing involve modifying one of these 3 key parameters to achieve their intended effect.

For ESCS systems consisting of a continuous roof and floor that sandwich a coal seam with even stiffness, the LMS (k_p) is equivalent to normal stiffness of the roof (k_R). In cases where the roof is considered "hard," indicating a higher elastic modulus (E_R), the k_R is elevated, resulting in a higher k_p. Consequently, meeting the required stiffness criterion becomes a challenge. This clash between stiffness theory and practical engineering experience remains unresolved within ESCS arrangements.

In contrast, for USCS systems consisting of a continuous roof and floor that sandwich a coal seam with an uneven stiffness distribution, the stiffness reduction function allows for a decrease in k_p, making it easier to meet the stiffness criterion. Although an increase in E_R results in a higher k_p, the increment in k_p for USCS is considerably smaller compared to ESBS. Simulation results indicate that parameters such as H_R, S_R, and K_H/K_L, in addition to E_R, can affect the value of k_p. Certain USCSs have $H_R S_R K_H/K_L$ values that are sufficiently large, effectively reducing k_p below the threshold stated in Equation (1). Even with an increase in E_R within a specific range, these USCSs continue to satisfy the stiffness criterion, thereby maintaining a high risk (r_I) of instability. In accordance with Equation (3), raising the E_R of specific USCSs with sufficiently larger $H_R S_R K_H/K_L$ values can lead to an increase in r_F while keeping the r_I constant, thereby resulting in an increase in the r_{CB}. This observation regarding USCS aligns with engineering expertise, which suggests a greater likelihood of coal bursts under the presence of a hard roof with higher E_R. Thus, USCS can explain why hard roofs and floors are more susceptible to coal bursts without contradicting the stiffness theory. Thus partially resolves the conflict between stiffness theory and practical engineering experience.

5. Further Discussion about USCS

5.1. Connection between USCS and Existing Mechanism Research Results about Coal Burst

Based on the cusp-type catastrophe theory, Pan Y.S. [16] highlighted that the occurrence of coal bursts is contingent upon the roof experiencing a sudden jump subsidence characterized by an adequate amplitude. The roof above the damaged coal mass is expected to sink, but the presence of surrounding undamaged coal mass provides support and inhibits further subsidence. In Figure 9, it can be observed that roof in HSZ of USCS exhibits an upper convex bending prior to the failure of the coal mass, and the subsidence of the roof after failure (ΔH_2) is considerably greater than that of the ESBS (ΔH_1). Based on Pan Y.S.'s viewpoint, it can be inferred that coal mass fails in HSZ of USCS is more likely to result in coal burst than ESCS.

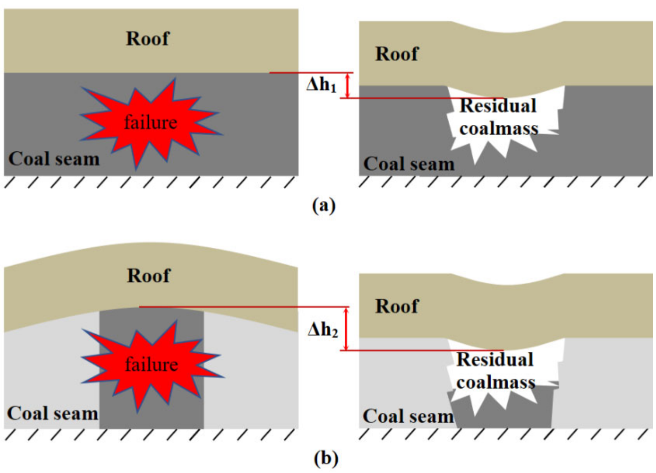

Figure 9. Roof subsidence after coal mass failure of ESCS and USCS. (**a**) Roof subsidence after coal mass failure of even stiffness coal seam structure; (**b**) Roof subsidence after coal mass failure of uneven stiffness coal seam structure.

Cook once said: "rock bursts often occur due to the violent failure of columnar rock units that are relatively isolated" [10]. These "relatively isolated columnar rock units" mentioned by Cook, similar to the "mine pillars" in Blake's description of stiffness theory [12], were previously understood by most researchers as coal pillar. However, these terms can also encompass columnar coal units with high NSC surrounded by coal mass with lower NSC. The HSZ of the USCS can be likened to a concealed coal pillar embedded within the solid coal, which is enclosed by LSZ. The contrasting stiffness levels result in disparate deformations and create the appearance of isolation in mechanical behavior for the HSZ amidst the LSZ. Similar to load-bearing column, the HSZ plays a crucial role in supporting the roof within a broader range than its own cross-sectional area. Once the coal mass of HSZ fails, it triggers significant stress adjustments and configuration changes within the coal mass-surrounding rock system, which may cause the significant sudden subsidence of the roof proposed by Pan Y.S. [16], and ultimately leading to coal bursts.

From an energy perspective, when coal mass of the ESBS fails, the energy released by the surrounding rock is the elastic deformation energy; Under the same conditions, when the coal mass in HSZ of USCS fails, the surrounding rock not only releases the same amplitude of elastic deformation energy, but also additionally releases the bending deformation energy of the roof and floors. Therefore, the failure of coal in HSZ of USCS is more likely to meet energy criterion, and according to energy theory, it also has a higher risk of coal burst.

Several scholars have emphasized the significant role of accumulating and releasing bending deformation energy in promoting coal burst incidents [3,4]. Nevertheless, it is challenging for the roof of ESCS to undergo bending. Consequently, a sufficient span of hanging roof is required in the goaf to amass an ample amount of bending deformation energy, often necessitating roof breakage to facilitate its release. In the main roadway or excavation tunnels, the hanging roof span is typically below 10 m. Although a thick and rigid roof can accumulate a substantial amount of bending deformation energy, It is unlikely to break under a 10-m span. Conversely, a soft or thin roof can fracture but fails to accumulate enough bending deformation energy to cause a coal burst. Therefore, while the assertion that bending deformation is released through roof fracture, leading to coal bursts, can account for coal bursts near the mining face, goaf pillars, and similar areas, it struggles to explain coal bursts occurring in the main or excavation roadways located far from the working face and goaf.

The "11.3" coal burst incident in 2011, which took place in the lower roadway of the 2121221 excavation working face at Qianqiu Coal Mine in Yima, Henan, China, occurred at a distance exceeding 200 m from the nearest goaf and more than 500 m from the closest mining working face [33]. Similarly, in 2016, the "8.15" coal burst occurred in the centralized track roadway of the 35000 mining district at Liangbaosi Coal Mine in Shandong, China, with the epicenter being 379 m away from the actively mined 35001 working face [34]. Notably, like the "6.5" coal bursts incident in 2014, which transpired in the main transportation roadway at Mengcun Coal Mine in Shaanxi, China, and the "11.13" coal burst at the auxiliary transportation roadway of the first panel of Gaojiabao Coal Mine, occurred at the excavation roadway [35].

These coal burst locations lacked sufficient span of suspended roof conditions, leading to limited accumulation of bending deformation energy on the roof. In areas with USCS, the uneven distribution of stiffness induces roof bending, allowing for the accumulation of bending deformation energy even in the absence of hanging roof conditions. When the coal mass in HSZ experiences failure caused by the pressure concentration effect of USCS, the roof will restore its bending deformation and release energy without suffering from roof breakage. Hence, employing the USCS to elucidate coal burst in main or excavation roadways that are distant from the working face and goaf presents notable advantages. In the previously mentioned instances of coal bursts, the lower roadway of the 21221 working face at Qianqiu Coal Mine, which experienced the "11.3" coal burst, passed through the combined zone of 2-1 coal and 2-3 coal, where the coal seam thickness displayed significant variations [33]. The "8.15" coal burst was characterized by the presence of a magmatic rock intrusion zone [34]. Based on previous analyses, all of these instances are classified as the HSZs of USCSs.

There are many possible structures in coal measure strata, and Qi Q.X. did not specify that there is only one type of structural factor, namely the stick-slip weak surface. As depicted in Figure 2, the occurrence of stick-slip leads to an increased steepness of the post-peak curve and an increase in the absolute value of $|\lambda_b|$, prompting the system to meet the stiffness criterion. Furthermore, the existence of weak surfaces diminishes the overall strength of the pressure bearer, further prompting the system to meet the failure criterion. Although the stick-slip weak surface structure and the uneven stiffness coal seam structure (USCS) promote the system's failure and stiffness criteria in different ways, both structures present higher risks of failure and instability compared to conventional coal seams, thus increasing the likelihood of coal bursts. Therefore, it can be used as a new coal burst structural factor in addition to the stick-slip weak surface structure.

5.2. Artificial USCS and Stiffness Perspective

Two extreme cases, Model 9 and Model 10, were simulated in the simple simulation of USCSs. Model 9 features the LSZs composed of ideal coal seam with an extremely low elastic modulus (EL = 0.1 Pa). Model 10 represents the scenario of a coal pillar and goaf with a continuous roof, achieved by removing the LSZs within Model 9. Figure 10 portrays the calculation of Mises stress distribution and deformation for both models.

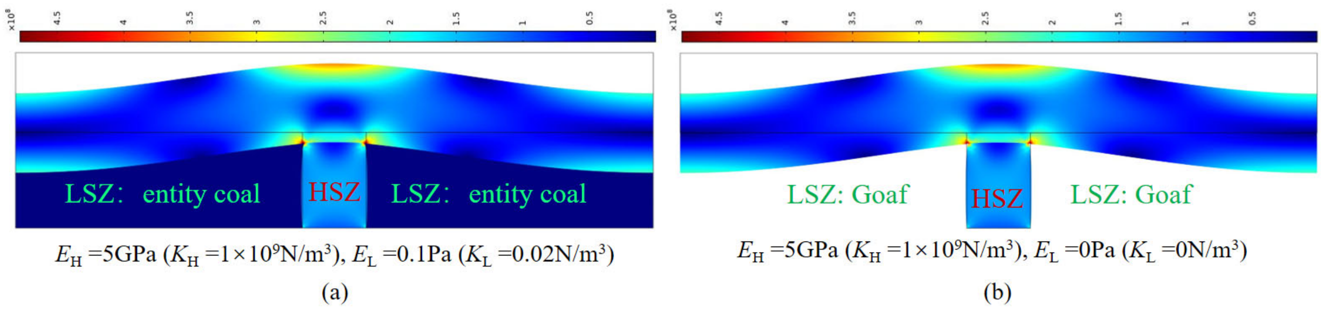

Figure 10. Comparison between Model 9 and Model 10 (stress unit: Pa): (**a**) Simulation results of Model 9; (**b**) Simulation results of artificial USCS (Model 10).

As shown in Figure 10 and Table 2, the simulation results of the model 9 and model 10 demonstrate a high level of consistency. Substituting the goaf in Model 10 with an ideal coal seam with a NSC close to 0 in Model 9 leads to negligible changes in stress distribution and deformation. This indicates that considering the goaf as a coal seam with an extremely low NSC is justified. Consequently, the combination of the entity coal and goaf can be seen as an uneven stiffness coal seam that, when coupled with the roof and floor, forms a distinctive USCS known as artificial USCS. The NSC of the excavated areas such as goafs and roadways in the coal seam reduces to 0, creating artificial LSZ. Conversely, the areas that haven't been excavated, such as entity coal and coal pillars, become relatively stiffer HSZs due to the retained original NSC. The stiffness contrast between the goaf and coal pillar is extremely significant, resulting in HSZ of artificial USCS bearing almost the entire overlying load.

From a stiffness perspective, the process of mining, excavation, slotting, drilling, failure and fracture development in coal seams can be seen as a process of reducing stiffness and then adjusting related parameters of existing USCS or creating new USCS. In this context, entity coal, coal pillars, and affected areas of remnant pillars represent the HSZs of artificial USCS. Conversely, the goaf, roadway, and affected areas of protective layer represent the artificial LSZs. Similarly, the HSZs of natural USCSs, such as thinning zones, bifurcating areas, and magmatic intrusion areas, can be regarded as coal pillars or isolated islands hidden in coal seam. Despite their apparent differences, both artificial and natural USCSs pose greater risks of failure and instability compared to conventional coal seams. This perspective provides a novel approach to understanding various engineering phenomena associated with coal burst. By applying stiffness theory and the relevant findings of USCS, valuable insights can be obtained, further elucidating these phenomena.

By mining the protective layers, the stress level exerted on the coal seam can be reduced, effectively mitigating the risk of coal burst. From a stiffness perspective, the combined presence of the protective layer, the protected coal seam, and the intermediate rock layers forms a composite coal seam with an uneven distribution of stiffness. The roof of the upper protective layer, the floor of the protected coal seam, and the composite coal seam, characterized by varying stiffness, collectively create an artificial USCS, as depicted in Figure 11. Drawing upon previous theoretical analysis and simulation results regarding USCSs, it is evident that the artificial LSZs, encompassing the affected areas of the protective layer, exhibit comparatively lower stress levels and a reduced risk of coal burst within the protected coal seam. In contrast, the artificial HSZs, including the affected areas surrounding the remnant coal pillar and the boundary of the protective layer, experience relatively higher stress levels and an increased risk of coal burst.

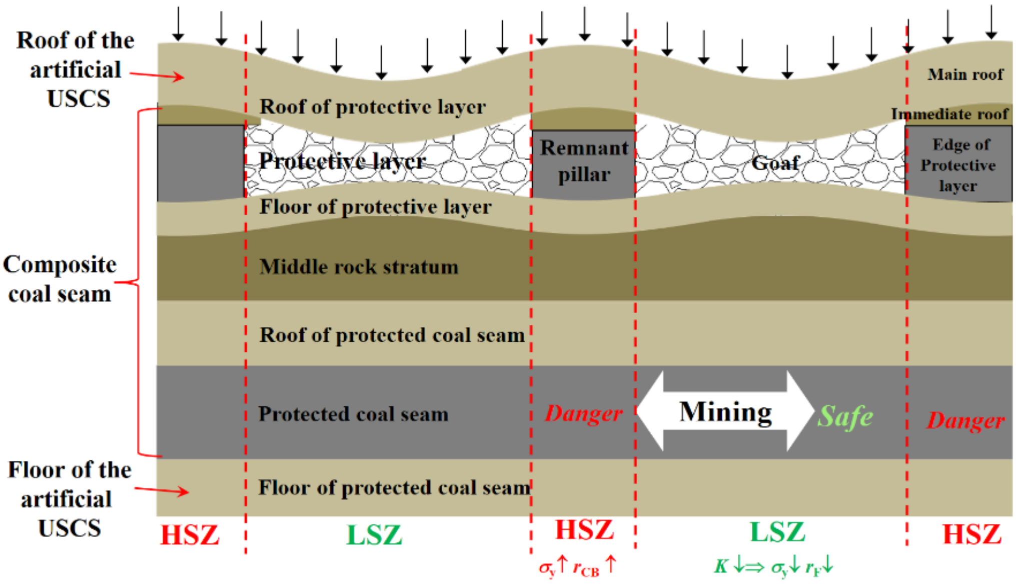

Figure 11. Artificial uneven stiffness coal seam structure produced by protective layer mining.

The majority of technical measures implemented to prevent and control coal burst or relieve pressure can be viewed as strategies for adjusting key parameters of the USCSs existing in coal measure strata. Measures such as coal seam slotting, blasting, water injection softening, large diameter pressure release drilling, and high pressure water jet cutting are capable of reducing the K_H. Conversely, actions such as grouting, goaf filling, and providing hydraulic supports, single props, anchor bolts can increase the K_L. For a specific rock stratum in the roof, roof cutting measures like directional hydraulic fracturing and deep hole blasting can decrease the area (S_R) of continuous roof and area (S_L) in LSZ. In practice, the roof and floor consist of multiple rock strata, making it challenging to carry out roof cutting measures for each individual layer in a multi-layered roof. Therefore, selecting a rock stratum with greater thickness or higher elastic modulus for fracturing or blasting among the various layers, instead of choosing randomly, can effectively reduce the thickness (H_R) or elastic modulus (E_R) of the continuous composite roof. The essence of these measures lies in reducing K_H, S_L (S_R), H_R, E_R, or increasing K_L, respectively. Tables 2 and 3 demonstrate that adjusting these key parameters of USCS can thereby achieving pressure relief and coal burst prevention.

Furthermore, the proximity of the roof cutting position to the HSZ-LSZ boundary plays a crucial role in the pressure relief effect. The closer the roof cutting position is to this boundary, the smaller the S_L (S_R), resulting in an enhanced pressure relief and coal burst prevention effect. Therefore, when selecting the roof cutting position, accurately determining the boundary between the LSZ and HSZ and identifying the specific stratum with a thicker or higher elastic modulus among the overlying rock layers is essential.

6. New Explanation of Engineering Phenomena Based on USCS

6.1. New Explanation of the Time-Delayed of Partial Coal Bursts

Certain coal burst accidents exhibit an unconventional characteristic known as the time-delayed property [35]. These coal bursts occur after a certain lag time following excavation disturbance. For instance, during the "11.3" coal burst incident at the 2121221 working face of Qianqiu Coal Mine, Yima in 2011, the location of the coal burst lagged behind the heading face of the excavation roadway by a distance ranging from 65 to 425 m [33]. Similarly, in 2017, the "2.3" coal burst transpired on the main roadway of Gaojiabao Coal Mine in Shaanxi during the mine's shutdown period for the Spring Festival [35]. It is possible that the coal burst resulted from mining disturbance prior to the shutdown period and only manifested during the Spring Festival shutdown period.

Excavation and unloading operations induce stress redistribution in the coal and rock mass around roadways, leading to localized fracture aeras known as loose rings or ring-shape broken rock zone, which consist of annular zones of broken rock distributed around the roadway [36]. The unloading effects of a developing loose ring can cause damage to the outer layer of coal and rock mass, gradually expanding the loose ring layer by layer, until the stable equilibrium is restored. Although the fractures resulting from the developing loose ring possess some elements of spontaneous and time-delayed characteristics, their weak burst intensity renders them incapable of causing coal bursts. Therefore, relying solely on the presence of a developing loose ring is insufficient to explain the time-delayed property of coal bursts. It is necessary to consider other factors, such as USCS, in conjunction with the loose ring.

The preceding analysis of USCS reveals that, similar to the effect of increasing static or dynamic loads, an increase in the value of $E_R H_R K_H S_L / K_L S_H$ or in NSC gradient between HSZ and LSZ can improve σ_{yH} and enable the coal mass in HSZ to reach the failure criterion. From a stiffness standpoint, the development of loose ring can reduce the NSC of the coal seam. When this process occurs in LSZ of USCS, the reduction in K_L can lead to a higher stress concentration and a lower LMS in HSZ, which promotes the satisfaction of failure criterion and instability criterion.

In the case of ESCS coal seams, minor disturbances like roadway expansion or loose ring development have limited impact on the stress field and hence are unlikely to cause coal bursts, since the load transfer caused by such disturbances is dispersed, as depicted in Figure 12a. In contrast, minor disturbances occur in LSZ of USCS may have significant effects on the stress field due to the pressure concentration function of USCS, which allows the loads from various parts of LSZ to converge congruously towards the HSZ, as shown in Figure 12b. Although the load transfer generated by a developing loose ring around a unit length of roadway is slight, a considerably lengthy roadway with a growing loose ring around it, or a close proximity between the HSZ and the growing loose ring, would result in a substantial increase in σ_{yH}, even leading to the failure criterion being met. Furthermore, compared to the occurrence of failure in coal seams of ESCS under similar conditions, failure of HSZ in USCS is more likely to result in coal bursts due to the stiffness reduction function of USCS.

In 2013, the "8.5" coal burst in the upper roadway of the 3302 excavation working face at Shandong Xingcun Coal Mine. The location of the coal burst was approximately 200 m away from the excavation heading face, surpassing the disturbance range of the excavation. Since 3302 working face was the first mining face, there was no other sources of disturbance in its vicinity. Assuming that the coal seam in close proximity to the site of the coal burst demonstrated a comparatively higher NSC, it combined with the surrounding coal seam, roof, and floor, forming an USCS, as illustrated in Figure 12b. Following the excavation of the roadway, the LSZ of the USCS can be categorized into three segments: the main coal section with a lower NSC, the loose ring, and the roadway. The excavation disturbance, along with the formation and progression of the loose ring, contribute to a decrease in K_L and an increase in σ_{yH}. As the excavation advanced 200 m away, the influence of excavation disturbance became negligible. Concurrently, the ongoing development of the loose ring around the newly excavated roadway led to a persistent reduction in the K_L and a subsequent rise in σ_{yH}. The σ_{yH} continued to escalate, eventually surpassing the critical threshold. Subsequently, this resulted in failure of the coal mass in the HSZ and triggered the occurrence of the coal burst.

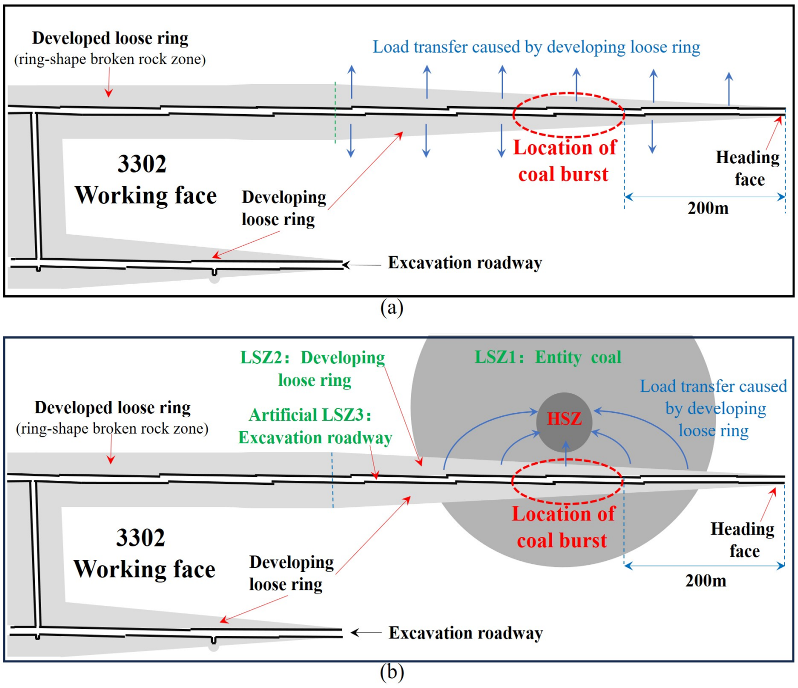

Figure 12. Two possible scenarios about "8.5"coal burst in Xingcun Coal Mine: (**a**) Development of loose ring occurs in ESCS coal seam; (**b**) Development of loose ring occurs in LSZ of USCS.

Dynamic loads or excavation disturbances are direct and easily detectable, while the development of the loose ring is gradual and difficult to detect. Consequently, a coal burst triggered by the interaction between USCS and developing loose ring exhibits a time-delayed or spontaneous property (without a specific disturbance source). The entire process of the loose ring develpment, from initiation to stability, can range from as short as 3–7 days to as long as 1–3 months [36]. For coal bursts with a lag time of less than 3 months, the combined effect of the loose ring development and USCS provides a plausible explanation.

6.2. New Explanation of the Inefficient Pressure Relief in Ultra Thick Coal Seam

From April to May 2014, continuous roof caving with strong burst intensity occurred at the heading face of a excavation roadway in China Xinjiang's Liuhuanggou Coal Mine [37]. The coal seam in close proximity to the incident site can be categorized as an ultra thick coal seam, given its substantial thickness of 36 m. To mitigate the issue, extensive large diameter pressure release drilling operations, with a depth of 25 m and a diameter of 120–150 mm, were conducted the front and both sides of the heading face. Regrettably, the desired pressure relief outcomes were not achieved. Consequently, adjustments were made to the initial plan, wherein a fan-shaped arrangement of 15 to 20 boreholes was implemented at the front to enhance compaction. Nonetheless, the mine pressure behavior was still strong during the excavation. Subsequently, a revised construction plan was devised and depicted in Figure 13 [37]. This revised approach involved the addition of two inclined pressure relief drillings, facing upwards and downwards respectively, resulting in effective control of the roof caving disaster.

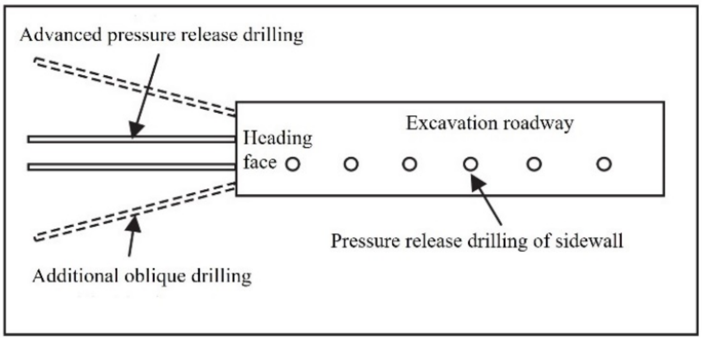

Figure 13. Final adjusted pressure relief plan for ultra thick coal seam in Liuhuanggou Coal Mine (Strike section of excavation road) [37].

From a stiffness standpoint, the strong mine pressure behavior observed at the heading face can be attributed to the coal seam with relatively higher NSC in close proximity to the heading face. Which forms an USCS in conjunction with the surrounding coal seam with lower NSC, as well as the roof and floors. The pressure concentration function leads to stress concentration in HSZ ahead of the heading face, and the stiffness reduction function amplifies the burst intensity of localized failure and triggers impactful roof caving incidents.

According to Table 3, pressure release drilling is a pressure relief and burst prevention measure that achieves the dual purpose of reducing stress concentration and improving LMS by reducing K_{H}. Drilling within HSZ can induce the formation of modified area, encompassing both the borehole and the adjacent fracture region, within which the average elastic modulus has decreased. The decrease in average elastic modulus of modified area within HSZ leads to a decrease in K_{H}. According to Table 3, the level of stress concentration in HSZ exhibits a positive correlation with the K_{H} value, so the effectiveness of pressure relief is positively correlated with the relative decrease in K_{H}. The relative decrease in K_{H} can be determined using Equation (14).

$$\begin{aligned}\frac{\Delta K_{\mathrm{H}}}{K_{\mathrm{H0}}} &= \frac{K_{\mathrm{H0}}-K_{\mathrm{H1}}}{K_{\mathrm{H0}}} = \left(\frac{E_{\mathrm{H0}}}{H_{\mathrm{c}}} - \left(\frac{E_{\mathrm{H0}}}{H_{\mathrm{c}}-h_d} \cdot \frac{E_{\mathrm{H1}}}{h_d}\right) / \left(\frac{E_{\mathrm{H0}}}{H_{\mathrm{c}}-h_d} + \frac{E_{\mathrm{H1}}}{h_d}\right)\right) / \frac{E_{\mathrm{H0}}}{H_{\mathrm{c}}} \\ &= \left(\frac{h_d}{H_{\mathrm{c}}} \cdot \left(\frac{E_{\mathrm{H0}}}{E_{\mathrm{H1}}} - 1\right)\right) / \left(\frac{h_d}{H_{\mathrm{c}}} \cdot \left(\frac{E_{\mathrm{H0}}}{E_{\mathrm{H1}}} - 1\right) + 1\right) = \left(\frac{E_{\mathrm{H0}}}{E_{\mathrm{H1}}} - 1\right) / \left(\frac{E_{\mathrm{H0}}}{E_{\mathrm{H1}}} - 1 + \frac{H_{\mathrm{c}}}{h_d}\right)\end{aligned} \tag{14}$$

where, K_{H0} is the initial normal stiffness coefficient (NSC) of the coal seam within HSZ prior to drilling, K_{H1} is the NSC subsequent to drilling. H_{c} is the thickness of the coal seam, E_{H0} is the elastic modulus of the coal. h_{d} is the thickness of the modified area generated by drilling, E_{H1} is the average elastic modulus of the modified area.

By examining Equation (14), it becomes evident that the pressure relief effect achieved through large diameter drilling technique displays a negative correlation with the thickness of the coal seam, but presents a positive correlation with the thickness (h_{d}) of the modified area formed subsequent to drilling. Consequently, under similar conditions, thicker coal seams yield a less favorable pressure relief effect when implementing large-diameter drilling. Zhang D.X. et al. [38] conducted a numerical simulation study to analyze the influence of coal seam thickness on the pressure relief effect of large-diameter drilling. Their findings affirmed that, with identical pressure relief drilling parameters, thin coal seams offer superior pressure relief effects compared to thick coal seams. These research results align consistently with Equation (14).

The inefficient pressure relief in ultra thick coal seams as the Liuhuanggou Coal Mine is primarily attributed to the reduction in pressure relief effect resulting from the significant thickness. While dense construction fan-shaped drilling can extend the pressure relief range, the increase in h_{d} (thickness of the low stiffness portion) is limited, leading to suboptimal pressure relief effects. Based on Equation (14), it becomes apparent that increasing h_d is necessary to enhance the pressure relief effect for ultra thick coal seams. Expanding the drilling diameter or increasing the number of boreholes in the normal direction can accomplish this, but in engineering practice, the latter is typically more feasible. The final adjusted pressure relief plan, as illustrated in Figure 13 involves achieving effective pressure relief for the ultra thick coal seam by adding boreholes in the normal direction.

6.3. New Explanation of the "Microseism Deficiency" Phenomenon before Coal Burst

During microseismic monitoring of the mining face, occasional observations of a phenomenon known as "microseism deficiency" have been made. This phenomenon signifies a significant decrease in both the frequency and energy of microseismic events during specific time periods or in certain areas [39,40]. The occurrence of a "microseism deficiency" phenomenon often indicates a high probability of coal burst, strong mine pressure behavior, or the emergence of high-energy microseismic events. For instance, in 2006, when the 1410 working face of Shandong Huafeng Coal Mine approached a remnant coal pillar in the lower protective layer, the extension of the microseismic event distribution area did not proceed as usual with the advancement of the working face. Instead, it was halted at a distance of 50 m ahead of the remnant pillar, resulting in a continuous reduction in the advancement fracture area. Then a coal burst occurred, characterized by an energy release of 2.2×10^7 J, once the working face exceeded the coal pillar [41]. Similarly, during a 5 day period from 4–8 October 2011, the frequency and energy of microseismic events in the 8935 fully mechanized caving working face of Yao Coal Mine in Xinzhou remained consistently lower than the average. Subsequently, on October 9th, a coal burst occurred, releasing an energy of 5.9×10^5 J [39]. In another case, the 31103 working face of Bayangaole Coal Mine in Inner Mongolia experienced a "microseism deficiency" period lasting 2–3 days during monitoring before and after 20 September 2017. This was followed by a high-energy microseismic event with an energy release of 1.1×10^5 J in the middle of the working face on 22 September, which fortunately did not cause serious damages due to its distance from the roadway [40]. Consequently, scholars have widely acknowledged the "microseism deficiency" phenomenon as a precursor feature of coal burst [39,40].

When the normal stress surpasses a specific critical threshold, weak sections within the coal mass undergo damage and subsequently release energy. If this released energy exceeds the threshold of the microseismic monitoring system, a microseismic event occurs. Generally, as stress levels increase, higher frequencies and energy levels of microseismic events are observed. Conversely, when the stress remains below the critical threshold, the coal sections encounter difficulties in releasing enough energy to reach the microseismic monitoring system's threshold. Consequently, the monitoring results indicate a scarcity of microseismic events.

As illustrated by the yellow line in Figure 14, the mining stress field undergoes movement as the working face progresses. Each point within the coal mass ahead of the working face typically undergoes a process wherein the normal stress gradually increases from the average pressure (P) to the peak value (σ_{ymax}), followed by a rapid decrease below P. Therefore, in the absence of notable variations across different positions within the coal mass, the microseismic events in the monitoring results should exhibit an even distribution. The occurrence of the "microseism deficiency" phenomenon indicates notable disparities among various positions within the coal seams.

As shown in Figure 14, if a fixed USCS is present within the entity coal ahead of the mining face, the artificial USCS generated due to mining operations will overlay with the fixed USCS to varying extents at different positions as the working face progresses. The superposition of two USCSs does not augment the total load, but rather redistributes stress, resulting in an increase of mining stress in HSZ and a decrease in LSZ. Previous analyses and simulation results indicate a positive correlation between the normal stress (σ_{yL}) in LSZ and the value of $K_L S_L / E_R H_R K_H S_H$. Moreover, the closer a position in LSZ is to the HSZ-LSZ boundary, the greater the reduction in stress relative to the average pressure (P).

If the fixed USCS has a sufficiently small $K_L S_L / E_R H_R K_H S_H$ value, a specific zone near the HSZ-LSZ boundary in LSZ may witness a significant reduction in normal stress, effectively preventing the actual stress after redistribution from reaching the critical threshold, even when the mining stress peaks in that zone. Prior to the overall failure occurring in HSZ, the frequency and energy of microseismic events within this specific zone will be notably lower than in conventional scenarios, leading to the designation of this zone as a "microseism deficiency" zone. As the working face progresses, there will be a "microseism deficiency" period when the high-stress section of the mining stress field traverses through this zone.

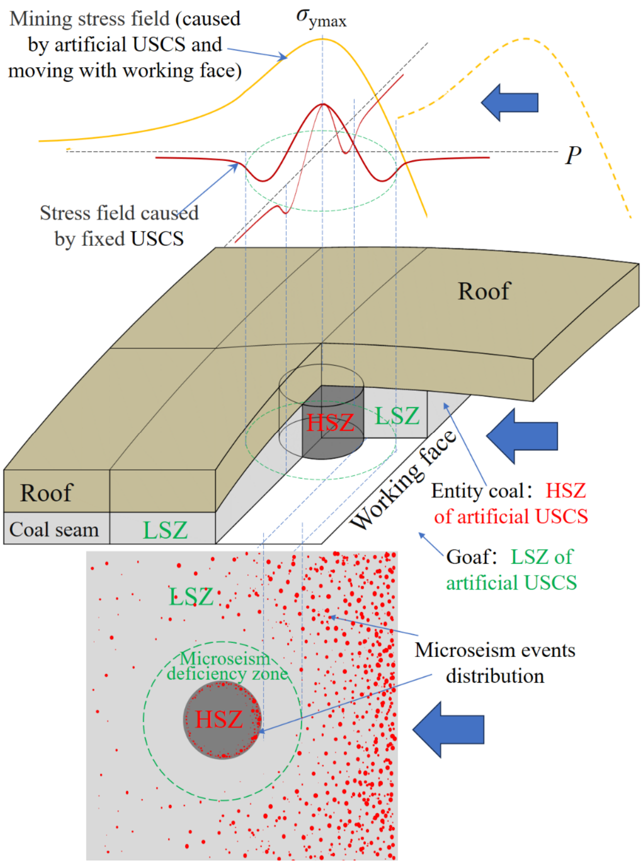

Figure 14. Microseism deficiency phenomenon caused by the dynamically superposition of moving artificial USCS (the mining face) and fixed USCS.

From an energy perspective, the HSZ of USCS acts as an energy storage device during the "microseism deficiency" period: the energy that should have been released by microseismic events under normal circumstances will be converted into compressive deformation energy of coal mass in HSZ. Considering the proximity of the "microseism deficiency" zone near the HSZ-LSZ boundary, the high-stress section of the mining stress field enters the HSZ of USCS after passing through this zone. As a result, there is a significant increase in the actual stress, which makes the HSZ highly vulnerable to failure. Once failure occurs in HSZ, the compressive deformation energy stored in HSZ during the "microseism deficiency" period will be released together with the bending potential energy of the roof, and its burst intensity will significantly exceed the failure of other parts in the entity coal. The energy of corresponding microseismic events will also be significantly higher than that of other microseismic events. If the HSZ of USCS is damaged when it is close to the mining space, it is likely to cause coal burst.

Figure 15 illustrates the distribution of microseismic events prior to and following the "9.9" impact that occurred in the 1410 working face of Huafeng Coal Mine in 2006 [41]. The composite coal seam, comprising the No.14 coal seam, the mined No.16 coal seam, and their intermediary rock strata, exhibits an uneven normal stiffness. Consequently, the composite coal seam, along with the roof of the No.14 coal seam and the floor of the No.16 coal seam, constitutes a fixed artificial USCS. The majority of the 1410 working face falls within LSZ, resulting in reduced stress and reduced risk (r_{CB}) of coal burst. However, the affected region of the underlying remaining pillar represents a HSZ, which escalates stress levels and increases the r_{CB}. Based on the analysis, the HSZ gives rise to the creation of a "microseism deficiency" zone with a width of approximately 50 m surrounding the remnant coal pillar. Consequently, the advancement of the 1410 working face in proximity to the remnant coal pillar leads to the occurrence of the "microseism deficiency" phenomenon, as depicted in Figure 15.

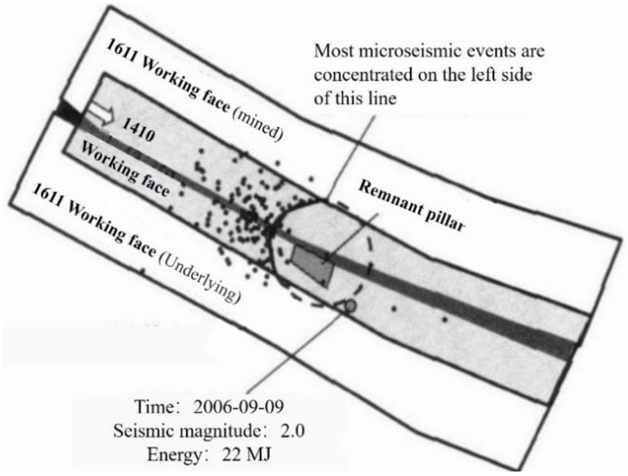

Figure 15. Microseismic events distribution before the "9.9" coal burst in Huafeng Coal Mine [41].

7. Conclusions

In this paper, Several often overlooked details of stiffness theory were clarified, and a qualitative evaluation formula for the risk of coal burst was provided. On this basis, a novel structure called uneven stiffness coal seam structure (USCS), which consists of high stiffness zone (HSZ), low stiffness zone (LSZ), and contiguous roof and floor, was proposed to reconcile the contrast between stiffness theory and engineering experience. Comparative analysis of the uneven stiffness coal seam under different roof conditions and examination of the simplified trisection model of the USCS were conducted. The findings revealed that the USCS exhibits two distinct functions, which can facilitate coal burst occurrence and affected by six key parameters. 6 groups of 14 simplified 2D models using COMSOL5.2 software was constructed based on controlled variable method to simulate different responses of the USCS with varying parameters under same working conditions. The main conclusions are as follows.

(1) The necessary condition for coal burst based on the stiffness theory include both failure criterion and stiffness criterion. Based on the two criteria of stiffness theory, a qualitative evaluation formula for the risk of coal burst is proposed: the probability of coal burst occurrence (r_{CB}) is the product of the probability of failure (r_F) and the probability of post-peak instability (r_I).
(2) The USCS exhibits pressure concentration function and the stiffness reduction function. The former promote the convergence of normal stress from LSZ to HSZ, thus raising the r_F of HSZ. The latter decreases the local mine stiffness (LMS), enabling the system to meet the stiffness criterion even with a hard roof, thus reconciling the contrast between the stiffness theory and engineering experience to some extent and increasing the r_I of HSZ. As a result of these two functions, the HSZ of USCS possesses a higher probability (rCB) of coal burst compared to onventional coal seam.
(3) The two functions of USCS are governed by 6 key parameters, such as: the elastic modulus (E_R) and thickness (H_R) of the roof, the NSC (K_H) and area (S_H) of HSZ,

the NSC (K_L) and area (S_L) of LSZ. The analysis indicated that σ_{yH} (normal stress in HSZ) is positively correlated with the value of $E_R H_R K_H S_L / K_L S_H$, the σ_{yL} is positively correlated with the value of $K_L S_L / E_R H_R K_H S_H$, the LMS ($k_p$) in HSZ is positively correlated with the value of $E_R K_L / K_H$. The simulation results validated the analysis results about USCS, and revealed that the variation in stress induced by the USCS is positively correlated with variation gradient of NSC between HSZ and LSZ, while the $\overline{K}_{pH}$ (average LMS per unit area in HSZ) is negative correlated with $H_R S_L S_H$.

(4) The USCS is associated with many existing theoretical research findings on coal burst. It offers a new way to partially reconcile the contradiction between engineering experience and stiffness theory, and provides a fresh approach to release bending elastic energy without roof breakage for energy theory. It also reveals the presence of a concealed coal pillar embedded within the solid coal, supporting Cook's proposition regarding "relatively isolated columnar rock units." Additionally, it identifies the HSZ a specific failure position that leads to increased roof subsidence, thereby aligning with Pan Y.S.'s assertion on the sufficient conditions for coal burst. Moreover, the USCS introduces a novel structural factor into "three-factors" mechanism. Consequently, the USCS serves as a valuable tool for integrating and harmonizing various existing theories on coal burst.

(5) Due to the pressure concentration function, the stiffness reduction function, and the characteristics of bending the roof under a uniform load, USCS offers distinct advantages in elucidating coal bursts induced by minor disturbances like roadway expansion or loose ring development, as well as coal bursts under hard roof conditions and those transpiring in the main or excavation roadways situated at a considerable distance from the working face and goaf.

(6) Relevant USCS findings can offer fresh insights into some engineering phenomena associated with coal burst: The goaf and roadway can be seen as coal seam with zero stiffness or LSZs of artificial USCSs, while the HSZs of USCSs prone to coal burst, such as thinning zones, bifurcating areas, magmatic intrusion areas, and remnant pillar affected areas, can be seen as concealed coal pillars embedded within the solid coal. A developing loose ring in LSZ increases the normal stress of the coal seam in HSZ, potentially leading to time-delayed coal bursts. Thicker coal seams may require larger borehole diameters or more boreholes to prevent inefficient pressure relief. Certain USCS can significantly reduce normal stress near the HSZ-LSZ boundary, thereby mitigating the frequency and energy of microseismic events within a specific range during mining operations.

Author Contributions: Conceptualization, T.T.; methodology, T.T., Z.D. and W.R.; formal analysis, T.T. and S.Z.; Investigation, T.T. and W.R.; writing-original draft preparation, T.T., Y.W. and Y.Z.; writing-review and editing, S.Z. and Z.D.; Visualization, T.T., W.R. and Y.W.; supervision, S.Z., Z.D. and W.L.; funding acquisition, T.T., Y.Z. and W.L. All authors have read and agreed to the published version of the manuscript.

Funding: This research was funded by Science and Technology Development Fund Project of China Coal Research Institute [grant No. 2021CX-II-11 & No. 2022CX-I-04 & No. 2023CX-I-06], Industry-University-Research Collaboration Project of China Coal Technology & Engineering Group [grant No. 2020-2-TD-CXY005], Open Fund Research Project of State Key Laboratory of Strata Intelligent Control and Green Mining [grant No. SICGM202106].

Institutional Review Board Statement: Not applicable.

Informed Consent Statement: Not applicable.

Data Availability Statement: All data generated or analyzed during this study are included in this published article.

Conflicts of Interest: The authors declare no conflict of interest.

References

1. He, M.C.; Miao, J.L.; Feng, J.L. Rock burst process of limestone and its acoustic emission characteristics under true-triaxial unloading conditions. *Int. J. Rock Mech. Min. Sci.* **2010**, *47*, 286–298. [CrossRef]
2. Lippmann, H. Mechanics of "bumps" in coal mines: A discussion of violent deformations in the sides of road-ways in coal seams. *Appl. Mech. Rev.* **1987**, *40*, 1033–1043. [CrossRef]
3. Qi, Q.X.; Dou, L.M. *Theory and Technology of Coal Bump*; China University of Mining and Technology Press: Xuzhou, China, 2008. (In Chinese)
4. Pan, Y.S.; Li, Z.H.; Zhang, M.T. Distribution, type, mechanism and prevention of rockbrust in China. *Chin. J. Rock Mech. Eng.* **2003**, *22*, 1844. (In Chinese)
5. Jiang, Y.D.; Pan, Y.S.; Jiang, F.X.; Dou, L.M.; Ju, Y. State of the art review on mechanism and prevention of coal bumps in China. *J. China Coal Soc.* **2014**, *39*, 205–213. (In Chinese)
6. Qi, Q.X.; Li, Y.Z.; Zhao, S.K.; Zhang, N.; Zheng, W.; Li, H.; Li, H.Y. 70 years development of coal mine rockburst in China: Establishment and consideration of theory and technology system. *Coal Sci. Technol.* **2019**, *47*, 1–40. (In Chinese)
7. Brauner, G. *Ground Pressure and Coal Bumps*; Li, Y.S., Translator; Coal Industry Press: Beijing, China, 1985. (In Chinese)
8. Cook, N.G.W.; Hoek, E.; Salamon, M.D.G. Rock Mechanics Applied to Study of Rockbursts. *J. S. Afr. Inst. Min. Metall.* **1966**, *66*, 435–528.
9. Cook, N.G.W. The failure of rock. *Int. J. Rock Mech. Min. Sci. Geomech. Abstr.* **1965**, *2*, 389–403. [CrossRef]
10. Cook, N.G.W. A note on rock bursts considered as a problem of stability. *J. S. Afr. Inst. Min. Metall.* **1965**, *65*, 437–446.
11. Salamon, M.D.G. Stability, instability and design of pillar workings. *Int. J. Rock Mech. Min. Sci. Geomech. Abstr.* **1970**, *7*, 613–631. [CrossRef]
12. Blake, W. Rockburst mechanics. *Q. Colo. Sch. Mines* **1972**, *67*, 1–64.
13. Kidybinski, A. Bursting liability indices of coal. *Int. J. Roc Mech. Min. Sci. Geomech. Abstr.* **1981**, *18*, 295–304. [CrossRef]
14. Zhang, M.T. Discussion on the mechanism of coal burst. *J. Fuxin Min. Inst.* **1985**, *4*, 65–72. (In Chinese)
15. Tang, C.A.; Xu, X.H. A cusp catastrophic model of rock unstable failure. *Chin. J. Rock Mech. Eng.* **1990**, *9*, 100–107. (In Chinese)
16. Pan, Y.S.; Zhang, M.T. The study of coal burst by catastrophe theory. *J. Fuxin Min. Inst.* **1992**, *11*, 12–18. (In Chinese)
17. Wang, S.Y.; Lam, K.C.; Au, S.K.; Tang, C.A.; Zhu, W.C.; Yang, T.H. Analytical and Numerical Study on the Pillar Rockbursts Mechanism. *Rock Mech. Rock Engng.* **2006**, *39*, 445–467. [CrossRef]
18. Qi, Q.X.; Shi, Y.W.; Liu, T.Q. Experimental study on stick slip instability mechanism of rockburst. *J. China Coal Soc.* **1997**, *21*, 34–38. (In Chinese)
19. Pan, J.F.; Ning, Y.; Mao, D.B.; Lan, H.; Du, T.; Peng, Y. Theory of rockburst star-up during coal mining. *Chin. J. Rock Mech. Eng.* **2012**, *31*, 586–596. (In Chinese)
20. Dou, L.M.; He, J.; Cao, A.Y.; Gong, S.Y.; Cai, W. Rock burst prevention methods based on theory of dynamic and static combined load induced in coal mine. *J. China Coal Soc.* **2015**, *40*, 1469–1476. (In Chinese)
21. Pan, Y.S. Disturbance response instability theory of rockburst in coal mine. *J. China Coal Soc.* **2018**, *43*, 2091–2098. (In Chinese)
22. Dou, L.M.; Tian, X.Y.; Cao, A.Y.; Gong, S.Y.; He, H.; He, J.; Cai, W.; Li, X.W. Present situation and problems of coal mine rock burst prevention and control in China. *J. China Coal Soc.* **2022**, *47*, 152–171. (In Chinese)
23. Gao, F.Q.; Kang, H.P.; Lou, J.F.; Li, J.Z.; Wang, X.Q. Evolution of Local Mine Stiffness with Mining Process: Insight from Physical and Numerical Modeling. *Rock Mech. Rock Eng.* **2019**, *52*, 3947–3958. [CrossRef]
24. Jaiswal, A.; Shrivastva, B.K. Stability analysis of the proposed hybrid method of partial extraction for underground coal mining. *Int. J. Rock Mech. Min. Sci.* **2012**, *52*, 103–111. [CrossRef]
25. Gu, R.; Ozbay, U. Numerical investigation of unstable rock failure in underground mining condition. *Comput. Geotech.* **2015**, *63*, 171–182. [CrossRef]
26. Liu, J.X.; Tang, C.A.; Zhu, W.C.; Yang, T. Rock-coal model model for studying the rockburst. *Chin. J. Geotech. Eng.* **2004**, *26*, 276–280. (In Chinese)
27. Li, J.Q.; Qi, Q.X.; Mao, D.B.; Wang, Y.X. Discussion on evaluation method of bursting liability with composite model of coal and rock. *Chin. J. Rock Mech. Eng.* **2005**, *24* (Suppl. S1), 4805–4810. (In Chinese)
28. Dou, L.M.; Lu, C.P.; Mu, Z.L.; Zhang, X.T.; Li, Z.H. Rock burst tendency of coal-rock combinations sample. *J. Min. Saf. Eng.* **2006**, *23*, 43–46. (In Chinese)
29. Gu, J.C.; Fan, J.Q.; Kong, F.L.; Wang, K.T.; Xu, J.M.; Wang, T. Mechanism of ejective rockburst and model testing technology. *Chin. J. Rock Mech. Eng.* **2014**, *33*, 1081–1089. (In Chinese)
30. Tan, Y.L.; Zhang, M.; Xu, Q.; Guo, W.Y.; Yu, F.H.; Gu, S.T. Study on occurrence mechanism and monitoring and early warning of rock burst caused by hard roof. *Coal Sci. Technol.* **2019**, *47*, 166–172. (In Chinese)
31. Hudson, J.A.; Crouch, S.L.; Faihturst, C. Soft, stiff and servo-controlled testing machines: A review with reference to rock failure. *Eng. Geol.* **1972**, *6*, 155–189. [CrossRef]
32. Hojem, J.P.M.; Cook, N.G.W.; Heins, C. Stiff, two meganewton testing machine for measuring the work-softening behaviour of brittle materials. *S. Afr. Mech. Eng.* **1975**, *25*, 250–270.
33. Qi, Q.X.; Zhao, S.K.; Zhang, Y.; Liu, J.; Li, H.T. *Ten Typical Accidents of Coal Mine Rockburst and Their Analysis*; Emergency Management Press: Beijing, China, 2021. (In Chinese)

34. Liu, S.H.; Pan, J.F.; Wang, S.W. Rock burst mechanism of heading roadway in thick coal seam in magmatic intrusion areas. *Chin. J. Rock Mech. Eng.* **1975**, *25*, 250–270. (In Chinese)
35. Pan, J.F.; Qi, Q.X.; Liu, S.H.; Wang, S.W.; Ma, W.T.; Kang, X.C. Characteristics, types and prevention and control technology of rock burst in deep coal mining in China. *J. China Coal Soc.* **2020**, *45*, 111–121. (In Chinese)
36. Dong, F.T. *Roadway Support Theory and Applied Technology Base on Broken Rock Zone*; China University of Mining and Technology Press: Xuzhou, China, 2001. (In Chinese)
37. Zhu, S.T.; Dong, X.K.; Jiang, F.X.; Wang, X.; Zhang, X.; Liu, X.; Jiang, Y.; Li, L.; Ning, Y. Failure mechanism of pressure relief with advance drilling in driving face of strong burst ultra thick coal seam in Liuhuanggou coal mine. *J. Min. Saf. Eng.* **2022**, *39*, 45–53.
38. Zhang, D.X.; Wang, X.Y.; Guo, W.Y.; Zhang, Y.Y.; Zhao, T.B.; Wu, Z.; Fang, H.Y.; Zhang, Q. The influence of coal seam thickness on the pressure relief and energy release mechanism of large-diameter drilling hole. *Coal Sci. Technol.* **2023**. Available online: http://www.cnki.net/KCMS/detail/detail.aspx?dbcode=CAPJ&dbname=CAPJLAST&filename=MTKJ20230724001&uniplatform=OVERSEA&v=iCC3s9gAi1tvWIUxT8hujp2fsfplHdrHToyRku8ib95SNhgwA8Mfhfu59Q-1g46r (accessed on 24 October 2023). (In Chinese/OL).
39. Zhao, Y.X.; Jiang, Y.D.; Wang, T.; Gao, F.; Xie, S.T. Features of microseismic events and precursors of rock burst in underground coal mining with hard roof. *J. China Coal Soc.* **2022**, *37*, 1960–1966. (In Chinese)
40. Zhao, S.K. Mechanism of force-structure cooperative prevention and control of deep hole roof pre-blasting for rock burst. *J. China Coal Soc.* **2021**, *46*, 3419–3432. (In Chinese)
41. Wang, C.W.; Jiang, F.X.; Wang, P.; Kong, L.H.; Sun, Q.G.; Sun, C.J.; Zhang, M. Microseismic events distribution characteristic and mechanism of rock bursting induced by a coal pillar. *J. China Coal Soc.* **2009**, *34*, 1169–1173. (In Chinese)